https://doi.org/10.1016/j.bioorg.2024.107163

Multi-targeting oligopyridiniums: Rational design for biofilm dispersion and bacterial persister eradication

Jiaqi Li [a,1], Yue Yu [a,1], Yu Zhou [a], Junfeng Song [a], Anming Yang [a], Min Wang [a], Youzhi Li [a], Muyang Wan [b], Chunhui Zhang [b], Huan Yang [c,*], Yugang Bai [a,*], Wing-Leung Wong [d,*], Huangsheng Pu [a,b,e,f,*], Xinxin Feng [a,*]

[a] Institute of Chemical Biology and Nanomedicine, State Key Laboratory of Chemo/Biosensing and Chemometrics, Hunan Provincial Key Laboratory of Biomacromolecular Chemical Biology, and School of Chemistry and Chemical Engineering, Hunan University, Changsha, Hunan 410082, China

[b] College of Biology, Hunan University, Changsha, Hunan 410082, China

[c] Xuzhou Key Laboratory of Laboratory Diagnostics, School of Medical Technology, Xuzhou Medical University, Xuzhou 221004, China

[d] State Key Laboratory of Chemical Biology and Drug Discovery, Department of Applied Biology and Chemical Technology, The Hong Kong Polytechnic University, Hung Hom, Kowloon 999077, Hong Kong, China Hong Kong Special Administrative Region

[e] College of Advanced Interdisciplinary Studies & Hunan Provincial Key Laboratory of Novel Nano Optoelectronic Information Materials and Devices, National University of Defense Technology, Changsha, Hunan 410073, China

[f] Nanhu Laser Laboratory, National University of Defense Technology, Changsha 410073, China

* Corresponding authors
E-mail address:
yanghuan2015@tmu.edu.cn (H. Yang)
baiyugang@hnu.edu.cn (Y. Bai)
wing.leung.wong@polyu.edu.hk (W.-L. Wong)
phs@nudt.edu.cn (H. Pu)
xinxin_feng@hnu.edu.cn (X. Feng)

[1] The authors are contributed equally in this study.

Abstract

The development of effective antibacterial drugs to combat bacterial infections, particularly the biofilm-related infections, remains a challenge. There are two important features of bacterial biofilms, which are well-known critical factors causing biofilms hard-to-treat in clinical, including the dense and impermeable extracellular polymeric substances (EPS) and the metabolically repressed dormant and persistent bacterial population embedded. These characteristics largely increase the difficulty for regular antibiotic treatment due to insufficient penetration into EPS. In addition, the dormant bacteria are insensitive to the growth-inhibiting mechanism of traditional antibiotics. Herein, we explore the potential of a series of new oligopyridinium-based oligomers bearing a multi-biomacromolecule targeting function as the potent bacterial biofilm eradication agent. These oligomers were rationally designed to be "charge-on-backbone" that can offer a special alternating amphiphilicity. This novel and unique feature endows high affinity to bacterial membrane lipids, DNAs as well as proteins. Such a broad multi-targeting nature of molecules not only enables its penetration into EPS, but also plays vital roles in the bactericidal mechanism of action that is highly effective against dormant and persistent bacteria. Our *in vitro*, *ex vivo*, and *in vivo* studies demonstrated that **OP_{c3}**, one of the most effective derivatives, was able to offer excellent antibacterial potency against a variety of bacteria and effectively eliminate biofilms in zebrafish models and mouse wound biofilm infection models.

Introduction

Microbial biofilm formation is now widely acknowledged as a major virulence factor in numerous localized chronic infections [1,2]. The resilience of biofilms against medical interventions primarily arises from their inherent resistance to conventional antibiotics and the host immune response [3,4]. This resistance is rendered by two critical features, namely biofilm matrix [5] and dormant/persistent bacterial populations[6]. The biofilm matrix, as a shared space for encased microbial cells, comprises a wide variety of extracellular polymeric substances (EPS), including polysaccharides, proteins, amyloids, lipids, and extracellular DNA (eDNA) [5,7]. The matrix, constituting ~ 90 % of the biofilm biomass, exhibits a viscoelastic nature that not only tethers cells within the biofilm, providing a protective shield, but also acts as a scaffold for the three-dimensional biofilm structure [8–10]. This structure leads to high impermeability to a wide range of chemicals, including antibiotics [4,11]. In many cases, antibiotics can only reduce biofilms but fail to eliminate the entire biofilm [12]. Additionally, bacterial cells in biofilm enter various states, including slow growth, cessation of growth, or dormancy, and these properties make them insensitive to antibiotics due to infrequent division [13]. Collectively, the formation of biofilm could lead to 10–1000 times greater antibiotic resistance than the corresponding planktonic bacteria [11,14,15], contributing to the recalcitrance and recurrent nature of such infections *in vivo* [15].

Current anti-biofilm strategies developed include inducing biofilm dispersal, targeting EPS, metabolic interference, and targeting dormant cells in biofilms [9]. Among which, biofilm-dispersal agents offer a promising treatment strategy because the EPS matrix can dynamically modulate chemical and nutrient gradients, and delineate pathogenic environments (such as acidic pH and hypoxia) that contribute to key virulence attributes including recalcitrance [9]. Biofilm dispersion is usually achieved by targeting essential EPS components such as protein targeting by flavonoids [16–19], DNA targeting by zwitterionic micellar [20] and exopolysaccharides targeting by PslG [21]. However, one of the significant drawbacks of biofilm dispersion is that the disperser cells, if they are not treated, are likely to translocate and seed infection in new areas. It ultimately leads to the spread of the initial infection. Therefore, regardless of their dispersed state, it remains vitally important in the clinical setting that dispersive or exogenous EPS degrading agents are administered alongside systemic antibiotics to avoid pathogen recolo- nization and, potentially, septicaemia. Nevertheless, as stated previously, regular antibiotics, a majority of which have growth-inhibiting mechanism of action, are ineffective against the dormant bacterial persisters in the biofilm. Therefore, a biofilm-dispersal agent having strong bactericidal

effects is highly desirable in biofilm eradication; however, it is mostly unachievable for a molecule or drug that can only target a single biomacromolecule of bacteria. We thus hypothesize that to design molecular drugs with multi-target ability in bacterial cells may be able to generate synergistic effects and enhance biofilm dispersion and bacterial persister eradication, despite this approach is challenging.

In the present study, to achieve the aim, we designed and synthesized a series of new oligopyridinium (**OP**)-based oligomers that possessed multi-target ability (with high affinity to three important bacterial biomacromolecules including membrane lipid, DNA and proteins), which enables its distribution throughout the biofilm matrix and within bacterial cells. This unique ligand design generates a "charge-on-back- bone" type alternating amphiphilicity topology (Fig. 1A). These oligomers display potent antimicrobial activity against actively growing bacterial cells and also eradicate the mature bacterial biofilm of *S. aureus*. Mechanistic investigations reveal that, $\mathbf{OP_{c3}}$, the best hit screened, has strong multi-targeting affinity to these biomacromolecules of bacteria. The penetration of $\mathbf{OP_{c3}}$ into the biofilm causes serious EPS disruption and that further facilitates the accumulation and potentiation of traditional antibiotics, such as Vancomycin, to kill the bacteria protected by biofilms. The triple-target mechanism of action of the oligomer also greatly impacts normal bacterial cell functions. It results in a bactericidal killing kinetic against dormant and persistent bacteria. The broad-spectrum nature of $\mathbf{OP_{c3}}$ in anti-biofilm activities is also demonstrated against the multidrug-resistant strain of *S. aureus* and other important pathogenic bacteria, such as *E. faecalis* and *E. coli*. Moreover, the *ex vivo* and *in vivo* studies reveal that $\mathbf{OP_{c3}}$ exhibits high anti-biofilm activity and efficacy in a fibroblast biofilm model, a zebrafish infection model and a mouse wound biofilm infection model. The results may indicate a therapeutic potential of these new oligopyridinium-based oligomers in treating biofilm-related infections.

Results and Discussion

Design and synthesis of oligopyridiniums with triple biomacromolecule targeting ability

We have previously developed a series of dual-targeted oligomers featuring a "charge-on-backbone" structure [22–27]. These oligomers, endowed with cationic properties from amidines and guanidine, exhibited potent antimicrobial effects. Notably, one specific oligoamidine displayed efficacy against bacterial biofilms by permeating EPS due to its rigid and "sword-like" structure [26]. Nonetheless, these com- pounds still displayed restricted EPS dispersion capabilities, possibly stemming from their insufficient binding affinity with EPS components. To address this limitation, in the present study, we conducted a comprehensive study to design a collection of oligomers with enhanced biomacromolecule binding affinity and aimed to facilitate biofilm dispersion and eliminate dormant bacterial persisters entrenched within the biofilm matrix. We identified the positively charged pyridinium cation that could be a promising building block for the construction of the multi-target oligomers that exhibited strong affinity for bacterial DNAs, proteins, and cell membranes, since the effects of pyridinium cations on DNA transfection, protein delivery, and membrane per- meabilization have been demonstrated in various studies [28–30]. For instances, Sharma *et. al.* engineered pyridinium-based surfactants for the generation of synthetic transfection systems [28]. Matos *et. al.* utilized pyridinium moieties to equilibrate protein charges, thereby enhancing their applicability in bioconjugation while preserving the effectiveness of antibody-drug conjugates [29]. Geng *et. al.* leveraged the membrane- permeable attributes of pyridine moieties to conceive and produce a highly effective antimicrobial polymer, in which the pyridine played a crucial role as a membrane-targeting component [30].

In the molecular design for novel oligopyridiniums as the potential antibacterial and anti-biofilm agents, our approach is to utilize cationic pyridinium moiety as the core scaffold to recognize and bind to DNA, proteins and membranes in live bacterial cells and biofilm EPS with high affinity. In addition, the linker module connecting the pyridinium units is an important factor of consideration for enhancing the bioactivity and controlling the cytotoxicity of a molecule [31]. We therefore utilized a "combinatorial condensation" approach to synthesize our oligomer through nucleophilic substitution reactions (Fig. 1B) and 24 oligopyr-idiniums were successfully obtained with high purity for this study (Figs. S1–S24). Furthermore, the molecular mass of these oligomers is controlled to be 5000 Da by approximately tuning reaction conditions (Fig. S25).

Antibacterial and anti-biofilm properties of oligopyridiniums

The newly obtained oligopyridiniums were first examined against a number of planktonic bacteria including *E. coli*, *A. baumannii*, *S. aureus*, *B. subtilis* and *E. faecalis* for their antibacterial potential. The results were shown in Table 1. It was found that substantial antimicrobial effects of the oligopyridiniums were observed against these bacterial pathogens including Gram-positive bacteria and Gram-negative bacteria. The minimum inhibitory concentration (MIC) value obtained was ranged from 0.5 to 8 μg/mL. With these supportive results, we further investigated the anti-biofilm effect of **OP**s against *S. aureus* biofilms and, as expected, a majority of these oligopyridiniums exhibited obvious anti- biofilm ability.

Among the **OP** series evaluated, we found that $\mathbf{OP_{c3}}$ showed the most robust antibacterial and anti-biofilm property. In the activity screening against *S. aureus*, *E. coli* and *E. faecalis* $\mathbf{OP_{c3}}$ exhibited good bactericidal activity, as indicated by the low MIC at 2 μg/mL (Table 1). Additionally, its anti-biofilm activity is evidenced by the low minimum biofilm inhibition concentration (MBIC) at 8 μg/mL and minimum biofilm eradication concentration (MBEC) at 16 μg/mL. The potency of $\mathbf{OP_{c3}}$ in antibacterial and anti-biofilm activity is markedly higher than the previously reported oligoamidine (**3a**) [26]. This observation suggests that $\mathbf{OP_{c3}}$ has high potential in eradicating biofilms formed by these pathogenic bacteria effectively. Considering these results obtained thus far, $\mathbf{OP_{c3}}$ is a promising candidate for conducting an in-depth mechanistic investigation.

$\mathbf{OP_{c3}}$ shows high affinity towards important biological targets of bacterial membrane lipid, protein and DNA in vitro

We next investigated the affinity of $\mathbf{OP_{c3}}$ for the important bacterial biomacromolecules including membrane lipids, proteins and DNA with a series of *in vitro* assays. To study binding affinity of $\mathbf{OP_{c3}}$ with bacterial cell membranes, we assessed its antibacterial activity in the presence of essential membrane [32,33]. As shown in Fig. 2A, the bactericidal activity of $\mathbf{OP_{c3}}$ against both Gram-negative and Gram-positive bacteria was significantly reduced after the addition of 128 μg/mL phosphatidylglycerol (PG) or Lipopolysaccharides (LPS), indicating that $\mathbf{OP_{c3}}$ has affinity towards PG and LPS. In contrast, standard antibiotics Kanamycin and Vancomycin are unaffected because both of them are not membrane targeting. The membrane-targeting property of $\mathbf{OP_{c3}}$ may facilitate the internalization and accumulation of the compound into bacterial cells. To assess whether $\mathbf{OP_{c3}}$ was bacterial DNA-targeting, we performed gel retardance, DNA dye replacement and exogenous DNA interference assays. In the gel retardance experiment, $\mathbf{OP_{c3}}$ manifested robust binding of DNA, decelerating their migration through the gel matrix (Fig. 2B and Fig. S26A). It is noteworthy that $\mathbf{OP_{c3}}$ exhibits a higher DNA binding affinity than **3a**. Upon adding 8 μg/mL $\mathbf{OP_{c3}}$ to the assay, about 65 % of DNA experienced retardation (Fig. S26B). However, for the **3a**-treated DNA, the retardation effect (13 % or less) was found much weaker than that of $\mathbf{OP_{c3}}$ under the same conditions, indicating that $\mathbf{OP_{c3}}$ exhibited a higher DNA binding affinity. The results also in accord with our oligo- pyridinium design rationale to improve DNA-targeting ability of the compound.

In the DNA dye replacement assay, Hoechst 33342, a well-known DNA staining dye, typically binds to double-stranded DNA (dsDNA) and extracellular DNA (eDNA) substrates and then generates blue fluorescence. In the competition assay, **OP$_{c3}$** was able to replace DNA-bound Hoechst 33342, as evidenced by a dose-dependent reduction in fluorescence signal (Fig. S26C and D). In addition, the presence of eDNA could mitigate antibiofilm activity of **OP$_{c3}$**, while the antibiotic Vancomycin that targets cell wall synthesis shows no effect upon adding eDNA (Fig. S26E and F). The results support that **OP$_{c3}$** may also bind to eDNA and induce polyplex formation and oligomer deactivation. How- ever, the non-DNA-targeting Vancomycin exhibits no such eDNA- induced effect.

To explore whether **OP$_{c3}$** had protein-interaction ability, we investigated its affinity for amyloid, a vital EPS matrix component that acts as a scaffold, conferring viscoelastic properties to the matrix [16,34,35]. In the assay, we utilized amyloid-specific dye Thioflavin T (ThT), which exhibited strong fluorescence upon binding to β-sheet structures formed in amyloid aggregates [20,35]. Quantitative evaluation revealed a remarkable reduction (70 %) in ThT fluorescence upon treating with **OP$_{c3}$** at 8 μg/mL, while only 30 % decreased when applying **3a** under the same treatment conditions (Fig. 2C). This result may support that **OP$_{c3}$** has stronger affinity to amyloid aggregates compared to **3a**. More importantly, the robust amyloid binding capacity of **OP$_{c3}$** may significantly contribute to its ability to disrupt the architecture of the EPS matrix.

OP$_{c3}$ achieves multi-site distribution in EPS matrix and bacterial cells throughout biofilm

OP$_{c3}$ is able to interaction with multiple bacterial bio- macromolecules including eDNA and EPS matrix such as amyloid and this property may enhance the permeability of the compound into bacterial biofilm matrix and also facilitate its accumulation in bacterial cells and the EPS network (Fig. 2D). To empirically validate this hypothesis, a derivative of **OP$_{c3}$** with a coumarin-labeled (**OP$_{c3}$**-Coumarin) was synthesized. The compound retains the same antibacterial efficacy as its parent compound **OP$_{c3}$**. **OP$_{c3}$**-Coumarin enables the direct visualization of **OP$_{c3}$** in a spatial distribution manner within the GFP- expressing *S. aureus* strain (GFP-*S. a*) biofilm. The confocal image shown in Fig. 2E illustrates the presence of **OP$_{c3}$**-Coumarin that gives blue fluorescence within the EPS matrix of the biofilm (indicated by a green circle). Furthermore, an intriguing overlap between the blue fluorescence of **OP$_{c3}$**-Coumarin and the green fluorescence of GFP-*S. a* (highlighted by an orange circle) suggests that **OP$_{c3}$** directly interacts with bacterial cells following the disruption of the EPS. Fluorescence profiling additionally provides a quantitative analysis of the dispersion pattern of **OP$_{c3}$**-Coumarin across the entire biofilm structure, as depicted in Fig. S27. A 3D-confocal imaging experiment was also performed. The result reveals that the blue fluorescence from **OP$_{c3}$**-Coumarin and the green fluorescence from GFP-*S. a* have a similar thickness (Fig. 2E). These results provide more experimental evidence that **OP$_{c3}$** may spread effectively throughout the entire depth of the GFP-*S. a* biofilm.

OP$_{c3}$ is a biofilm dispersing agent with antibiotic sensitizing activity

As previously mentioned, we demonstrated visually the distribution of **OP$_{c3}$** within the EPS, through its interaction with eDNA and amyloid proteins of EPS matrix. To observe a direct effect on dispersion of mature biofilm, we imaged the biofilm morphology with scanning electron microscopy (SEM). As depicted in Fig. 3A and Fig. S28A, the results demonstrate that **OP$_{c3}$** causes a significant dispersion of the EPS and bacterial cells compared the untreated sample. In contrast, the impact of Vancomycin on the dispersion of biofilm matrix was comparatively mild as the EPS connection between bacterial cells was obvious. Delving deeper into the SEM analysis, we also found a distinct transformation in the morphology of the biofilm bacteria subsequent to exposure to **OP$_{c3}$**. This transformation was marked by a shift from their rounded state to fragmented forms, characterized by a noticeable reduction in diameter and compromised cell membranes (Fig. 3A, 32 μg/mL **OP$_{c3}$**).

We are also interested in comparing the biofilm dispersion ability of

OP$_{c3}$ and **3a**, since **OP$_{c3}$** is presumed to have a better activity due to its stronger binding affinity toward bacterial biomacromolecule, which we have demonstrated in Fig. 2A–C. Quantitative comparison of biofilm dispersion was

performed with 3D confocal microscopy, which deter- mined the thickness of biofilm layer. These results suggest that GFP-*S. a* biofilm could be able to grow to a thickness of 10–14 mm within 48 h in the untreated control group (Fig. 3C, Untreated). However, after a treatment with **OP$_{c3}$** at 64 μg/mL, the biofilm thickness was found decreased to 6–8 μm, whereas the **3a**-treated group showed a reduction to approximately 9 μm only (Fig. 3B–C and Fig. S28B). We also note that, beyond the variation in thickness, the dispersion of the biofilm is notably greater following the treatment with **OP$_{c3}$**, as GFP-*S. a* appears more extensively separated. In contrast, the biofilm treated with **3a** retains a clustered configuration for GFP-*S. a*, as imaged in Fig. 3C and quantified in Fig. 3D.

The dispersion of bacteria cells is particularly important in enhancing the effectiveness of antibacterial treatments, as the dispersed bacterial cells are more susceptible to antimicrobial agents. This is verified by testing the synergistic interaction between Vancomycin and **OP$_{c3}$** or **3a**, in the eradication of mature GFP-*S. a* biofilm. The combi- nation treatment of **OP$_{c3}$** and Vancomycin, as depicted in Fig. 3E, demonstrates a potent synergistic antibacterial effect against GFP-*S. a* biofilms. Specifically, the combination of **OP$_{c3}$** at 8 μg/mL with Vancomycin at 8 μg/mL yields a 3.5-log reduction in bacterial CFU (colony-forming units), a striking contrast to the mere 1.5-log and 0.5-log de- creases exhibited by the individual agents. This outcome suggests that **OP$_{c3}$** treatment effectively disrupts the EPS structure, consequently, it facilitates the accumulation of Vancomycin for killing bacterial cells. By adeptly exposing bacterial cells, it renders them being more susceptible to the lethal effects of antibiotics. Conversely, the combination of **3a** with Vancomycin at the same concentration displays equivalent biofilm reduction as compared with the individual agent and it markedly lowers than the impact achieved by the **OP$_{c3}$**-Vancomycin combination (Fig. 3F).

Macromolecule targeting by OP$_{c3}$ and its efficacy in eradicating dormant/persistent bacteria without inducing resistance

Apart from the effects on the biofilm matrix, the elevated affinity of **OP$_{c3}$** for biological macromolecules may induce several detrimental outcomes on bacteria. Firstly, the lipid binding affinity of **OP$_{c3}$** com- promises bacterial membrane integrity and functionality. Fig. 4A illustrates that the zeta potential of *E. coli* and *S. aureus* bacteria transitions from negative to positive as increasing the concentration of **OP$_{c3}$**, indicating an electrostatically interaction of compound with negatively charged bacterial membranes. Moreover, the bacterial envelope also experiences significant damage due to the attraction of **OP$_{c3}$** to amphiphilic phospholipid lipids, as evidenced in SEM images of actively growing bacteria shown in Fig. 4B. The lytic action of **OP$_{c3}$** on mem- branes increases bacterial cell permeability and that may facilitate the entry of the membrane-impermeable propidium iodine (PI) dye, which subsequently binds to DNA in the bacteria and results in red fluorescence that can be quantified by flow cytometry. When comparing **OP$_{c3}$**-treated Gram-negative bacterium *E. coli* and Gram-positive bacterium *E. faecalis* with the untreated control group, as depicted in Fig. 4C, a notable in- crease of PI fluorescence was observed. This indicates a severe disruption on the function of bacterial membrane that acts as a permeability barrier. The disruption of permeability barrier may further facilitate the entry of **OP$_{c3}$** to cells. Using *S. aureus* and DiSC$_3$(5) probe (3,3′-dipro- pylthiadicarbocyanine iodide), a dye that fluoresces intensely when the membrane potential collapses, we conducted a cytoplasmic membrane depolarization assay. Upon treatment with **OP$_{c3}$**, we observed a substantial increase in fluorescence, suggesting that membrane disruption plays a role in the bactericidal effect of **OP$_{c3}$** (Fig. S29A).

OP$_{c3}$ upon internalized may actively bind directly to the crucial intracellular target DNA [36]. To test the hypothesis, bacterial cells (*A. baumannii*) were incubated with **OP$_{c3}$**-Coumarin. Confocal micro- scope images reveal a colocalization of **OP$_{c3}$**-Coumarin (4 μg/mL) staining with Acridine Orange (AO), a nucleoid-specific staining dye. This colocalization may support a direct evident that a DNA-targeting mechanism of **OP$_{c3}$** in bacterial cells (Fig. 4D). The disruption of permeability barrier may further facilitate the entry of **OP$_{c3}$** to cells. In contrast, in NIH/3T3 cells (mammalian cells), **OP$_{c3}$**-Coumarin does not enter the nucleus. The exclusion of **OP$_{c3}$** from the nucleus of mammalian cells significantly mitigates its cytotoxicity toward the cells. It further supports the distinctive capacity of **OP$_{c3}$** for selective disrupting bacterial membranes. The extensive perturbation of bacterial membranes and DNA

functions result in an ultrafast bactericidal kinetics exhibited against a range of bacterial species, as indicated by the results shown in Fig. S29B–D. Furthermore, this process stimulates the inherent generation of reactive oxygen species (ROS), a well-documented bactericidal mechanism of antibiotics [37,38], as demonstrated in Fig. 4E.

Firstly, we calculated the electrostatic surface potential (ESP) of **OP$_{c3}$** [39] to reveal the distribution of its positive charges and hydrophobic regions (Fig. S30A). This property allows the molecule to interact with biomolecules through electrostatic or hydrophobic interactions. From the analysis of EPS for lipid and DNA [40], shown in Fig. S30B-C, both DNA and lipid carry negative charges and have hydrophobic regions. Given the negatively charged protein surfaces, **OP$_{c3}$** may engage in electrostatic interactions with proteins [35]. We conducted DNA docking simulations with **OP$_{c3}$** using a fragment of **OP$_{c3}$** and dsDNA and the results showed that a minor groove binding was suggested (Fig. S31), which was found similar to many amidine-based DNA binders [41].

These multifaceted mechanisms underpin the capacity of **OP$_{c3}$** in effectively eliminating bacteria of varied lifestyles, which included those in dormant and persistent states, prevalent constituents within bacterial biofilms [42]. Bacterial dormancy is a universal survival strategy adopted to elude environmental threats, including antibiotics [43]. In the context of dormancy, where cells were cultured under nutrient- deficient conditions (DMEM-10 % FBS) to suppress bacterial growth [44], the MIC of **OP$_{c3}$** measured was 0.5 μg/mL, which was a 16-fold improvement over the MIC of Vancomycin (8 μg/mL) (Fig. 4F). It is because Vancomycin, which targets cell wall biosynthesis [45], suffers significant inactivation due to the pronounced reduction in biosynthetic and metabolic activities characteristic of dormant bacteria.

Beyond dormancy, bacterial biofilms also harbor persister cells, which exhibit remarkable multidrug tolerance [46]. Upon treating a bacterial culture of 10^9 CFU/mL GFP-*S. a* with Vancomycin for 6 h, a population of persistent cells was generated [46]. Subsequent addition of **OP$_{c3}$** at varying concentrations led to a striking outcome that all persister cells (8 Log CFU) were sterilized by **OP$_{c3}$** at 32 μg/mL within 2 h (Fig. 4G: 0—10 h), showcasing a rapid and consistent killing kinetics to both actively growing bacteria and dormant bacteria. In contrast, Vancomycin failed to eliminate persisters even at concentrations up to 64 × MIC.

The efficacy **OP$_{c3}$** against antibiotic-tolerant cells marks a significant advancement over the majority of conventional antibiotics. This observation reinforces the notion that **OP$_{c3}$** may exert its function through an unconventional mechanism that could target multiple macromolecules in the bacterial cells. Thus, it may overcome common resistance determinants while exhibiting minimal susceptibility to resistance evolution (Fig. 4H and Fig. S32). Our results reveal that **OP$_{c3}$** retains its antimicrobial effectiveness over 20 days despite a modest MIC increase. In contrast, the traditional antibiotics, such as Gentamicin and Ciprofloxacin, displayed a 32 ~ 128 folds increase in the initial mini- mum inhibitory concentrations (MICs) during progressive resistance evolution. This resilience underscores the multi-targeting nature of **OP$_{c3}$** in suppressing major resistance mechanisms.

Interestingly, there was no detectable resistance evolution to **OP$_{c3}$** in *E. coli* (Fig. S32). The variability in resistance evolution across bacterial species presents an intriguing question for future research into the underlying mechanisms governing evolutionary response.

Antibiofilm efficacy of OP$_{c3}$ against various S. Aureus strains and other pathogenic bacteria

The capability of microbes to form biofilms exhibits a significant disparity among diverse bacterial strains, influenced by genetic variations, surface structures, and physiological attributes—all of which impact their biofilm-forming propensity [47]. Consequently, acknowledging this diversity is paramount when assessing the effects of drugs or interventions on bacterial biofilms. Our aforementioned results high- light the proficiency of **OP$_{c3}$** in eradicating a GFP-*S. a* model strain and elucidate the multi-macromolecule targeting mechanism responsible for EPS dispersion and elimination of dormant/persistent cells. On the basis of these understanding, we further investigated the therapeutic potential of **OP$_{c3}$** across various *S. aureus* strains and other pathogenic bacteria. Our selection encompassed a standard methicillin-resistant *S. aureus* strain (MRSA), USA300, and two additional clinical *S. aureus*

isolates (*S. a*-1, *S. a*-2) with multidrug resistance (Table S1). By comparing with the untreated group, despite Vancomycin exhibits heightened sensitivity against certain bacterial strains (e.g. *S.a*-1), it falls short of completely eradicating bacteria within the biofilm, even at concentrations up to 128 μg/mL (Fig. 5A, e.g. *S.a*, *S.a*-2, *S.a*-USA300). This residual bacterial presence may promote recurrent infections. In contrast, **OP_{c3}** exhibits consistent competence in thoroughly eliminating all biofilm-associated bacteria.

Apart from *S. aureus*, clinically relevant bacteria such as *E. faecalis* and *E. coli* are also proficient in rapidly forming biofilms on tissues or implanted medical devices post-infection, making them substantial contributors to persistent and recurrent infections [48,49]. To evaluate the impact of **OP_{c3}** on these biofilms, we conducted tests and observed an MBEC of 32 μg/mL and an MBIC of 4 μg/mL for *E. coli*. Conversely, ampicillin, despite it showed high efficacy against actively growing bacteria, exhibited no influence on biofilms (Fig. 5B). For *E. faecalis*, **OP_{c3}** at a dose of 32 μg/mL achieved complete bactericidal effect against the biofilm, surpassing the effectiveness of a much higher Vancomycin dosage (128 μg/mL) (Fig. 5C). These findings underscore that, even within intricate environments and the presence of multiple bacterial strains, **OP_{c3}** still maintains its capacity to obstruct mature biofilm formation and destruction. This reaffirms the efficacy and the broad- spectrum nature of its multi-targeting functionality.

***Ex vivo* and *in vivo* assessments for the therapeutic potential of OP_{c3} against biofilm-associated infections**

The *ex vivo* and *in vivo* studies to evaluate the therapeutic potential **OP_{c3}** in treating biofilm-related infections were also performed. To assess biocompatibility on red blood cells, we conducted hemolytic toxicity tests on **OP_{c3}**. The results depicted in Fig. S33 reveal no in- stances of hemolysis at therapeutic concentration. Next, cytotoxicity experiments were conducted using mouse embryonic fibroblast cells (NIH/3T3) within concentrations ranged from 0 to 128 μg/mL. In the presence of 8 μg/mL **OP_{c3}**, the cell viability was found exceeding 60 % (Fig. S34). It is noteworthy that the MIC of **OP_{c3}** against *S. aureus* was 1 μg/mL. These findings underscore its potential as a promising candidate for further exploration in biomedical applications, showcasing a promising selectivity between antibacterial activity and biocompatibility. Moreover, an *ex vivo* fibroblast biofilm infection model that simulates the chronic wound environment conducive to biofilm development was established for the study. As depicted in Fig. 6A, the introduced GFP-*S. a* causes biofilm formation on fibroblast surfaces over time. The mature biofilms distorted the morphology of fibroblast cells. However, the treatment with 4 μg/mL **OP_{c3}** proved profoundly effective as it completely eradicated bacteria from the cell surface and the fibroblasts were restored to their normal state.

We further evaluated the toxicity of **OP_{c3}** using a zebrafish model and 100 % survival rate was observed. The result may support a low or mild toxicity of the compound (Fig. 6B). Encouraged by the results, we extended the investigation to the potential of **OP_{c3}** for treating bacterial infections *in vivo*. By employing a zebrafish infection model, animals were intraperitoneally infected with 10^8 CFU of *S. aureus*. After 30 min of infection, the zebrafish was treated with either PBS, 10 mg/kg of **OP_{c3}**, or Vancomycin (Fig. 6C). The **OP_{c3}** treated group exhibited a 60 % survival rate within 10 h, demonstrating its considerable bactericidal effects in zebrafish and its potential as a rescue treatment (Fig. 6D).

OP_{c3} displays a strong anti-biofilm efficacy in *in vivo* wound biofilm infection models

Encouraged by the promising anti-biofilm activity of **OP_{c3}** demonstrated in *in vitro* experiments, we next evaluated its efficacy in a clinically relevant *S. aureus* infected murine wound model. *S. aureus* is a prevalent pathogen in biofilm-mediated infections [50]. We utilized an established splinted excisional wound model in which a defined surface wound was created on the dorsal skin and subsequently infected with 10^8 CFU of *S. aureus* to enable robust biofilm formation [51] (Fig. 6E). Mice were divided into different treatment groups by independently administering **OP_{c3}** (10 mg/kg, 60 μL) topically applied to the wound site, Vancomycin (10 mg/kg, 60 μL) as a positive topical antibiotic control, sterile PBS vehicle (equal volume to **OP_{c3}**and Vancomycin groups) at the wound site.

Over the 7-day treatment course, parameters including bacterial burden within wound beds, clinical observations of mouse activity, quantitative wound area for healing progress monitoring, and body weight were evaluated. Notably, topical **OP$_{c3}$** treatment resulted in a significant 1.5-log reduction in bacterial load after just 1 day compared to PBS vehicle control (Fig. 6F). This rapid antibiofilm effect was maintained over 7 days, as shown by longitudinal quantification of bacterial loads in Fig. S35A-F. In these panels, each subfigure depicts a specific day post-wounding during topical **OP$_{c3}$** administration. Across the treatment period of 1–7 days, bacterial counts remained markedly suppressed by **OP$_{c3}$** compared to PBS vehicle. These findings demonstrate a potent and sustained biofilm-disrupting capability of topical **OP$_{c3}$** *in vivo*.

Furthermore, macroscopic wound healing kinetics were accelerated with **OP$_{c3}$** treatment versus PBS controls (Fig. 6G). Quantitative wound area measurements revealed more rapid wound area reduction in **OP$_{c3}$**-treated mice. Additionally, the endpoint of complete re-epithelialization was achieved earlier than PBS controls, indicating the beneficial effects of **OP$_{c3}$** on tissue repair processes in addition to its antibiofilm activity. Importantly, systemic toxicity of **OP$_{c3}$** on mice was not observed, as indicated by no adverse effects on body weight (Fig. S35G) and/or mouse health/activity relative to PBS upon subcutaneous injection at a distant site (Fig. S35H). Taken together, these *in vivo* findings support that **OP$_{c3}$** may exhibit strong efficacy against *S. aureus* wound biofilm infections and maintain excellent *in vivo* biocompatibility. **OP$_{c3}$** enables both accelerated wound healing and biofilm disruption and thus it could be further advanced for preclinical development as a novel antibiofilm therapeutic.

The *ex vivo* and *in vivo* studies provide experimental evidence to support that **OP$_{c3}$** could be a promising antimicrobial for combating biofilm-related infections. The efficacy of the compound in eradicating biofilms and its favorable safety profile in zebrafish models and epidermal wound infection models encourage further explorations for its therapeutic applications in higher level animal studies and antimicrobial coatings for medical devices.

Conclusion

In brief, this study extensively examined a range of novel pyridinium-based oligomers. It showcased the significant impact of pyridiniums in boosting binding affinity with biomacromolecules. This enhancement, in turn, reinforced EPS penetration and facilitated a bactericidal mode of action. The best derivative screened from this study, **OP$_{c3}$**, demonstrated the potent antibacterial and anti-biofilm activity across *in vitro* and *ex vivo* settings against the clinically important bacteria. It also showed potential as an *in vivo* rescue treatment for bacterial infections in zebrafish models and mouse wound biofilm infection models. Although being out of scope for this report, we envision that through additional chemical modification, diversification and screening, along with pharmacodynamic and pharmacokinetic studies, and with a more comprehensive assessment of potential side effects—particularly the risk of carcinogenicity and mutagenicity—this poly-cationic oligomer has the potential to evolve into even more promising candidates for tackling bacterial infections associated with biofilms.

Experimental Section

Materials

Chemical reagents

All solvents and reagents were purchased from Adamas Reagent (Shanghai, China), Sigma-Aldrich (USA), Macklin Chemical (Shanghai, China) and Leyan (Shanghai, China).

Biological reagents

Genomic DNA Mini-Extraction Kit (Universal, Spin Column, D0063) were purchased from Beyotime Biotech. Deoxyribonucleic acid from herring sperm (eDNA) was purchased from Sigma-Aldrich. Plasmid DNA pCold-ctxm-15 was a kind gift from Prof. Jing Huang. Dulbecco's modified Eagle's medium (DMEM, SH30022.01) and fetal bovine serum (FBS, 13011–8611) were purchased from HYCLONE® and TIANHANG Biotech. Water was generated using a Milli-Q water purifier. Genomic DNA of *S. aureus* was extracted from *S. aureus* Newman strain using the Genomic DNA Mini-Extraction Kit.

Bacteria strains and cell lines

The following bacteria were obtained from the American Type Cul- ture Collection (ATCC, Manassas, VA): *E. coli* (K12, ATCC 29425);
S. aureus Newman strain (ATCC 25904); *S. aureus* USA300 (ATCC BAA- 1717); *A. baumannii* (Bouvet and Grimont, ATCC 19606); *B. subtilis* from subsp. subtilis (Ehrenberg) Cohn (ATCC 6051); *E. faecalis* (Andrewes and Horder) Schleifer and Kilpper-Balz (ATCC 19433). *S. aureus* harboring a GFP-expression plasmid (GFP- *S. a*) is a kind gift from Prof. Hang Xing from Hunan University. All bacteria strains were confirmed by 16S ribosomal DNA sequencing. Murine embryonic fibroblast cell line NIH/3T3 (ATCC CRL-1658) were purchased from ATCC.

Instrumentation

Nuclear Magnetic Resonance (NMR). NMR spectra were recorded using a Bruker Avance II 400 MHz spectrometer equipped with an autosampler. The data was processed in MestReNova 6.1 and aligned/ annotated in Adobe Illustrator CC or Microsoft Paint of Windows 10.

Analytical Gel Permeation Chromatography (GPC). Gel permeation chromatography (GPC) analyses were performed on a Waters system equipped with a Waters 515 isocratic pump and a Waters 2414
refractive index detector. Separations were performed at 40 ˚C using an aqueous solution of $NaNO_3$ (0.01 M) as the mobile phase.

Scanning Electron Microscopy (SEM). SEM experiments were conducted on a Hitachi S-4800 scanning electron microscope. Bacteria sample were gold-plated before they were observed on SEM.

Flow Cytometry Study Flow cytometry studies were detected on a Becton Dickinson Accuri C6 Plus instrument. The green fluorescence was detected with an excitation of 488 nm and an emission of 533 +/-30 nm. The red fluorescence was detected with an excitation of 488 nm and an emission of 585 + -30 nm. The fluorescence signal was quantified by geometric mean. The data was processed in FlowJo, aligned and annotated in Adobe Illustrator CC.

Confocal Microscopy. Fluorescence microscope images were ac- quired using a Nikon Eclipse Ti2-E Laser Confocal Microscope. For blue fluorescence, wavelength was set at 405 nm for excitation. For green fluorescence, wavelength was set at 488 nm for excitation. For red fluorescence, wavelength was set at 561 nm for excitation.

General methods for the synthesis of oligomers

The dipyridine (1 mmol) and dibromide (1 mmol) compounds were dissolved in a 10 mL acetonitrile solution and then were react at 70 ◦C for 1 h. After reaction, the solution was transferred to a 50 mL centrifuge tube and 30 mL acetone was added to the solution. Precipitate was then formed. The mixture was centrifuged at 8000 rpm for 5 min. The supernatant was discarded. The obtained solid was repeatedly washed with acetone (30 mL) for four times by applying the same separation procedures. The solid was collected and dried under vacuum.

Yield and characterization for **OP$_{a1}$**: The isolated yield for the com- pound was 77 %. ^{1}H NMR^{1}H NMR (400 MHz, Deuterium Oxide) δ 9.06 (d, J = 6.0 Hz, 4H), 8.47 (d, J = 6.3 Hz, 4H), 2.17 (s, 4H).

Yield and characterization for **OP$_{a2}$**: The isolated yield for the compound was 72 %. ^{1}H NMR (400 MHz, Deuterium Oxide) δ 9.03 (d, J =6.2 Hz, 4H), 8.46 (d, J = 6.6 Hz, 4H), 4.67 – 4.60 (m, 4H), 2.10 (d, J =7.8 Hz, 4H), 1.51 (d, J = 14.0 Hz, 2H).

Yield and characterization for **OP$_{a3}$**: The isolated yield for the com- pound was 78 %. ^{1}H NMR (400 MHz, Deuterium Oxide) δ 9.02 (d, J = 6.0 Hz, 4H), 8.44 (d, J = 6.4 Hz, 4H), 4.63 (d, J = 7.8 Hz, 4H), 2.01 (s,4H), 1.41 (s, 4H).

Yield and characterization for **OP$_{a4}$**: The isolated yield for the com- pound was 78 %. ^{1}H NMR (400 MHz, Deuterium Oxide) δ 9.00 (d, J = 5.9 Hz, 4H), 8.43 (d, J = 5.9 Hz, 4H), 4.65 – 4.56 (m, 4H), 2.00 – 1.92 (m, 4H), 1.30 (s, 8H).

Yield and characterization for **OP$_{a5}$**: The isolated yield for the com- pound was 78 %. ^{1}H NMR (400 MHz, Deuterium Oxide) δ 9.12 (d, J = 3.9 Hz, 4H), 8.58 (d, J = 5.9 Hz, 4H), 6.42 (s, 2H), 5.47 (s, 4H).

Yield and characterization for **OP$_{a6}$**: The isolated yield for the compound was 75 %. ^{1}H NMR (400 MHz, Deuterium Oxide) δ 9.06 (d, J =5.5 Hz, 4H), 8.45 (d, J = 6.1 Hz, 4H), 7.51 (d, J = 7.7 Hz, 4H), 5.87 (s,4H).

Yield and characterization for **OP$_{a7}$**: The isolated yield for the compound was 54 %. ^{1}H NMR (400 MHz, Deuterium Oxide) δ 9.07 (d, J= 6.1 Hz, 4H), 8.46 (d, J = 6.0 Hz, 4H), 7.66 (s, 1H), 7.49 (s, 3H), 5.88 (s, 4H).

Yield and characterization for **OP$_{a8}$**: The isolated yield for the com- pound was 52 %. ^{1}H NMR (400 MHz, Deuterium Oxide) δ 9.14 (d, J = 6.4 Hz, 4H), 8.63 (d, J = 6.2 Hz, 4H), 7.62 (d, J = 4.5 Hz, 2H), 7.35 (d, J= 4.7 Hz, 2H), 6.18 (s, 4H).

Yield and characterization for **OP$_{b1}$**: The isolated yield for the compound was 77 %. ^{1}H NMR (400 MHz, Deuterium Oxide) δ 8.65 (d, J= 6.5 Hz, 4H), 7.88 (d, J = 6.2 Hz, 4H), 4.52 (s, 4H), 3.29 (s, 4H), 2.02 (s, 4H).

Yield and characterization for **OP$_{b2}$**: The isolated yield for the compound was 78 %. ^{1}H NMR (400 MHz, DMSO-d_6) δ 9.06 (d, J = 5.8 Hz, 4H), 8.14 (d, J = 6.0 Hz, 4H), 4.61 – 4.46 (m, 4H), 3.32 (s, 4H), 1.90 (s, 4H), 1.34 (s, 6H).

Yield and characterization for **OP$_{b3}$**: The isolated yield for the compound was 79 %. ^{1}H NMR (400 MHz, DMSO-d_6) δ 9.09 (d, J = 6.5 Hz, 4H), 8.17 (d, J = 6.2 Hz, 4H), 4.57 (s, 4H), 1.90 (s, 4H), 1.30 (s, 8H).

Yield and characterization for **OP$_{b4}$**: The isolated yield for the compound was 77 %. ^{1}H NMR (400 MHz, DMSO-d_6) δ 9.09 (d, J = 6.5 Hz, 4H), 8.17 (d, J = 6.3 Hz, 4H), 4.64 – 4.49 (m, 4H), 1.90 (s, 4H), 1.30 (s, 8H).

Yield and characterization for **OP$_{b5}$**: The isolated yield for the compound was 78 %. ^{1}H NMR (400 MHz, DMSO-d_6) δ 9.09 (d, J = 6.3 Hz, 4H), 8.23 (d, J = 6.1 Hz, 4H), 6.27 (s, 2H), 5.36 (s, 4H), 3.38 (s, 4H).

Yield and characterization for **OP$_{b6}$**: The isolated yield for the compound was 74 %. ^{1}H NMR (400 MHz, Deuterium Oxide) δ 8.74 (d, J= 6.1 Hz, 4H), 7.92 (d, J = 6.4 Hz, 4H), 7.47 (s, 4H), 5.76 (s, 4H), 3.35 (s, 4H).

Yield and characterization for **OP$_{b7}$**: The isolated yield for the compound was 72 %. ^{1}H NMR (400 MHz, Deuterium Oxide) δ 8.68 (d, J= 6.3 Hz, 4H), 7.87 (d, J = 6.1 Hz, 4H), 7.51 (s, 1H), 7.44 – 7.32 (m, 3H),
5.69 (s, 4H), 3.28 (s, 4H).

Yield and characterization for **OP$_{b8}$**: The isolated yield for the compound was 77 %. ^{1}H NMR (400 MHz, Deuterium Oxide) δ 8.64 (d, J= 6.2 Hz, 4H), 7.93 (d, J = 6.3 Hz, 4H), 7.47 – 7.42 (m, 2H), 7.13 – 7.05 (m, 2H), 5.87 (s, 4H), 3.34 (s, 4H).

Yield and characterization for **OP$_{c1}$**: The isolated yield for the com- pound was 72 %. ^{1}H NMR (400 MHz, Deuterium

Oxide) δ 8.60 (d, J = 6.2 Hz, 4H), 7.83 (d, J = 6.2 Hz, 4H), 4.50 (s, 4H), 2.93 (d, J = 7.2 Hz, 4H), 2.00 (s, 6H).
Yield and characterization for **OP$_{c2}$**: The isolated yield for the com- pound was 74 %. ^{1}H NMR (400 MHz, DMSO-d_6) δ 9.11 (d, J = 6.2 Hz, 4H), 8.12 (d, J = 6.3 Hz, 4H), 4.61 (t, J = 7.4 Hz, 4H), 2.98 (s, 4H), 2.05 (dt, J = 54.3, 7.8 Hz, 6H), 1.35 (s, 2H).
Yield and characterization for **OP$_{c3}$**: The isolated yield for the compound was 78 %. ^{1}H NMR (400 MHz, DMSO-d_6) δ 9.10 (d, J = 6.2 Hz, 4H), 8.10 (d, J = 6.1 Hz, 4H), 4.60 (t, J = 7.8 Hz, 4H), 2.97 (t, J = 7.9 Hz, 4H), 2.12 (t, J = 7.9 Hz, 2H), 1.93 (s, 4H), 1.36 (s, 4H).
Yield and characterization for **OP$_{c4}$**: The isolated yield for the com- pound was 75 %. ^{1}H NMR (400 MHz, Deuterium Oxide) δ 8.54 (d, J = 6.2 Hz, 4H), 7.76 (d, J = 6.3 Hz, 4H), 4.38 (t, J = 7.5 Hz, 4H), 2.88 (t, J = 5.6 Hz, 4H), 2.03 (dt, J = 13.5, 6.8 Hz, 2H), 1.83 (s, 4H), 1.19 (s, 8H).
Yield and characterization for **OP$_{c5}$**: The isolated yield for the com- pound was 76 %. ^{1}H NMR (400 MHz, Deuterium Oxide) δ 8.60 (d, J = 6.1 Hz, 4H), 7.85 (d, J = 6.3 Hz, 4H), 6.16 (s, 2H), 5.15 (s, 4H), 2.93 (t, J= 7.7 Hz, 4H), 2.09 (q, J = 8.1 Hz, 2H).
Yield and characterization for **OP$_{c6}$**: The isolated yield for the com- pound was 72 %. ^{1}H NMR (400 MHz, Deuterium Oxide) δ 8.68 (s, 4H), 7.88 (d, J = 5.9 Hz, 4H), 7.47 (d, J = 4.9 Hz, 4H), 5.72 (d, J = 5.1 Hz, 4H), 3.02 – 2.90 (m, 4H), 2.19 – 2.05 (m, 2H).
Yield and characterization for **OP$_{c7}$**: The isolated yield for the com- pound was 74 %. ^{1}H NMR (400 MHz, Deuterium Oxide) δ 8.64 (d, J = 6.3 Hz, 4H), 7.82 (d, J = 6.3 Hz, 5H), 7.54 – 7.31 (m, 5H), 5.67 (s, 4H), 2.91 (t, J = 7.8 Hz, 4H), 2.06 (p, J = 8.0 Hz, 2H).
Yield and characterization for **OP$_{c8}$**: The isolated yield for the compound was 77 %. ^{1}H NMR (400 MHz, Deuterium Oxide) δ 8.58 (d, J= 6.2 Hz, 4H), 7.86 (d, J = 6.3 Hz, 4H), 7.50 – 7.42 (m, 2H), 7.18 – 7.09 (m, 2H), 5.84 (s, 4H), 3.00 – 2.90 (m, 4H), 2.14 – 2.02 (m, 2H).

Antimicrobial assays

Minimum inhibitory concentration (MIC) measurement

MIC test was conducted using a standard microdilution broth method [52]. An overnight starter culture of bacteria in CAMHB was diluted 1000-fold in fresh CAMHB media, and grown at 37 ◦C to reach an $OD_{600\ nm}$ of approximately 0.3. This log-phase culture was diluted in fresh CAMHB broth to generate the working solution containing 5 × 10^5 CFU/ mL bacteria. **OP$_{c3}$** diluted with working solution to specific starting concentrations, and was added to a total volume of 200 μL into the first row. Plates were incubated at 37 ◦C, shaking at 220 rpm, for 16–24 h. The $OD_{600\ nm}$ values were measured to determine MIC values. Experiments were carried out in triplicate or more. **OP$_{c3}$**'s antimicrobial activity under different conditions was performed as described above, with the following culture medium CAMHB (pH = 6.0, 6.5) and CAMHB plus 10 % FBS.

Minimum biofilm inhibitory concentration (MBIC) measurement

GFP-*S. a* were cultured to mid-logarithmic growth phase in CAMHB at 37 ◦C and 220 rpm and then were diluted in BM2 medium to 5 × 10^7 CFU/mL, as calculated and converted from the bacterial optical density at 600 nm. 100 μL of this suspension was added to each well of a 96-well polystyrene microplate. Solutions without bacteria were included in each plate as negative controls. Drugs were added to the wells, serially diluted, and incubated at 37 ◦C without agitation for 24 h (or the indicated time periods in the case of kinetic measurement) to allow biofilm formation. The suspension containing planktonic bacteria was subsequently removed and then the wells were washed 3 times with 1 × PBS to remove residual planktonic bacteria. 100 μL of sterile 1 × PBS was then added to each well containing bacterial biofilm. The biofilm was then dispersed with 15 min of ultrasound at 40 Hz (Branson). The released bacterial load was determined by plating serial ten-fold dilutions on agar plates. The agar plates were then incubated overnight at 37 ◦C. The colonies were then counted to determine bacterial CFU. MBIC was defined as the

minimum concentration that inhibits formation of biofilm. Experiments were carried out in duplicate.

Minimum biofilm eradication concentration (MBEC) measurement

GFP-*S. a* were cultured until mid-logarithmic growth phase in CAMHB at 37 ◦C and 220 rpm and then were diluted in BM2 medium to 5 × 10^7 CFU/mL, as calculated and converted from the bacterial optical density at 600 nm. 100 μL of this suspension was added to each well of a 96-well polystyrene microplate. Solutions without bacteria were included in each plate as negative controls. Plates were incubated at 37 ◦C without agitation for 24 h to establish biofilm. After 24 h, the suspension containing planktonic bacteria was subsequently removed and the wells were washed 3 times with 1 × PBS to remove residual planktonic bacteria. The drug solution was diluted to the desired con- centration in BM2 medium by two-fold serial dilution, and then was added into each well containing bacterial biofilm. Plates were incubated at 37 ◦C without agitation for 24 h (or the indicated time periods in the case of kinetic measurement). The colony counting method used was the same as that in MBIC. MBEC was defined as the minimum concentration that completely eradicates the mature biofilm. Experiments were conducted in duplicate.

Biomacromolecule affinity assays

Lipid interference on MIC

An overnight culture of *E. coli* and *S. aureus* were diluted to a final concentration of 5 × 10^5 CFU/mL with CAMHB respectively, which were supplied with 128 μg/mL LPS or PG and used as a working solution. The procedure of the MIC assay was the same as described above.

Gel retardance assay

DNA was incubated with the compounds of interest for 30 min at 25 ◦C in PBS buffer (10 mM, pH 7.4). For plasmid pCold-ctx-m-15, the mixture was electrophoresed on a 1 % agarose gel with Gel red (2 μg/ mL) for 40 min. The shift in DNA bands was visualized and imaged under ultraviolet light using ChemiScope 6100 (Clinx). The DNA binding ability was analyzed through Grayscale analysis using ImageJ software.

Fluorescence titration experiment of Hoechst-DNA binding

This titration experiment was performed in PBS (pH 7.4) at 37 ◦C. pCold-ctx-m-15 (10 μg/mL) and Hoechst (8 μg/mL) were mixed and incubated for 30 min at 37 ◦C, and the plasmid-dye mixture was added compounds of different concentrations. The mixtures were incubated at 37 ◦C for 1 h to reach equilibrium. The fluorescence intensity of Hoechst in each mixture before and after **OP_{c3}** incubation was measured on a fluorometer.

The K_d value determined for Hoechst is 5.6 × 10^{-8} M. The K_i value determined for **OP_{c3}**-DNA interaction is calculated as follows:

$$K_i = \frac{IC_{50}}{1 + \frac{[Ligand]}{K_d}}$$

Anti-biofilm activity test under interference of eDNA

The experimental method is the same as the MBIC or MBEC experimental method mentioned above. The difference is that different concentrations of eDNA were added to the working solution.

Thioflavin t (ThT) fluorescence assay

To investigate the interaction between proteins and **OP_{c3}**, a thioflavin T (ThT) amyloid fibril assay was performed [53]. Five hundred microliters of ThT (26 M) were added to a well after *S. aureus* biofilm growth and exposure to micelles for 120 min. Subsequently, ThT was removed and 1 mL of PBS was added and pipetted vigorously in each well to detach the remaining biofilms and to homogenize the samples. Fluorescence in each well was measured using

an excitation wavelength of 440 nm and emission at 485 nm on a microplate reader. Micelle interaction with amyloidosis proteins was calculated as

$$Amyloid\ interaction(\%) = \frac{I_0 - I}{I_0} \times 100\%$$

in which I_0 is the ThT fluorescence of biofilm before micelle exposure and I is the ThT fluorescence of biofilm after micelle exposure. Accordingly, maximal interaction of amyloidosis proteins was 100 %. Each assay was carried out in triplicate.

Determination of OP_{c3}-Coumarin within biofilm

*Synthesis of **OP_{c3}**-Coumarin*

OP_{C3} (1 mmol) and 7-hydroxycoumarin (0.2 mmol) were added to a 10 mL acetonitrile solution and reacted at 70 ◦C for 1 h. After reaction, the purification and separation for the final products procedures applied were same as for **OP** series described in General Methods.

Fluorescence microscopy imaging of compounds distributions within biofilm

The general protocols for MBEC determination were applied with **OP_{c3}-Coumarin**, except that biofilm formation on a glass coverslip that was induced by placing the coverslip into a well of a sterile 12-well plate containing 1 mL GFP-*S. a* at 5×10^7 CFU/mL in BM2. After treatment, the glass coverslip was washed three to four times with PBS to remove planktonic bacteria.

The biofilm samples were imaged using inverted fluorescence microscopy or confocal fluorescence microscopy, where a Nikon Eclipse Ti2-E Laser Confocal Microscope was utilized to acquire images of green fluorescence with 488 nm excitation, and biofilm thickness was quantified by NIS-Elements Imaging Software.

Biofilm dispersing mechanism assay

SEM imaging of biofilm disruption

The glass coverslip preparation method described in the above. was applied for SEM imaging, with the following modifications for sample processing: the biofilm-containing coverslip was fixed in 2 % glutaraldehyde overnight at 4 ◦C. The samples were then dehydrated with a series of ethanol solutions (30 %, 50 %, 70 %, 90 % and 100 % in Milli-Q purified water) and sputter coated with gold for observation using a Hitachi S-4800 field emission scanning electron microscope.

Imaging of 3D biofilm

The experimental procedure was the same as described in the above. except that unlabeled **OP_{c3}** or 3a was used and drug treatment time was 48 h.

Synergistic assay of compounds with Vancomycin

The biofilm formation procedure followed the protocol outlined in the above. **OP_{c3}** or 3a at indicated concentration was introduced into the biofilm and incubated at 37 ◦C without agitation for 24 h. Following this incubation period, the wells were washed three times with 1 × PBS. Subsequently, vancomycin was added to the biofilm and incubated again at 37 ◦C without agitation for another 24 h. The biofilm was then dispersed with 15 min of ultrasound at 40 Hz (Branson). The released bacterial load was determined by plating the dispersed biofilm culture on agar plates following an overnight incubation at 37 ◦C.

Antimicrobial mechanism assay

Zeta potential measurement

E. coli K12 and *S. aureus* were cultured in CAMHB at 37 ◦C overnight, and diluted 40-fold in fresh CAMHB and incubated at 37 ◦C for 3 h, followed by washing with HEPES (40 mM, pH 7.4) for 3 times. The *E. coli* K12 and *S. aureus* were re-suspended in HEPES at density of 0.15 OD_{600nm}, and compounds of interest at different concentrations were added into the bacteria suspension. The mixtures were incubated at 37 ◦C for 2 h, followed by standing at room temperature for 1 h. Zeta potentials were measured on a Malvern Zetasizer Nano ZSP zetasizer.

SEM morphological study of bacteria

GFP-*S. a* growing in exponential phase were used and the suspension was incubated with the $\mathbf{OP_{c3}}$ at different concentration for 3 h. The bacterial suspension without any treatment was used as the negative control. After the treatment, the solution was centrifuged (1500 g, 10 min) to remove the supernatant. The bacteria were fixed after overnight incubation at 4 ◦C with PBS containing 2.5 % glutaraldehyde. Following the same sample preparation method as described previously in the above, the morphology of GFP-S. a before or after the treatment with $\mathbf{OP_{c3}}$ was observed under a Hitachi S-4800 scanning electron micro- scope (S-4800, Japan).

Bacterial membrane permeability assay

Propidium iodide was used as the fluorescent dye to evaluate integrity of bacterial membranes [54]. A stationary-state culture of

E. coli and *E. faecalis* was washed with PBS 3 times, then re-suspended to a working concentration (OD_{600nm} = 0.1) containing propidium iodide (100 μM). $\mathbf{OP_{c3}}$ were added at the indicated concentrations. The samples were incubated at 37 ◦C for 2 h. Cells with red fluorescence analysis was performed immediately by using flow cytometry (E_x = 488 nm, E_m = 585 ± 40 nm). In all cases, 1×10^4 events were counted.

Cytoplasmic membrane depolarization assay

Mid-log bacterial cells were harvested by centrifugation at 5000g for 5 min at room temperature and resuspended using assay buffer (5 mM HEPES and 20 mM glucose (pH 7.4)). The suspension was diluted 10- fold in assay buffer to reach a final concentration of 2×10^7 CFU/ml.

$DiSC_3(5)$ (0.4 μM) was then added followed by a 1-hour incubation at room temperature to allow quenching of $DiSC_3(5)$. One hundred microliters of the above bacteria suspension with $DiSC_3(5)$ was added into each well of a 96-well white microplate, and compounds of interest were added into the wells at different concentrations. The fluorescence intensity (E_x = 620 nm, E_m = 670 nm for $DiSC_3(5)$ dye) for each well was monitored for 30 min using a plate reader (Tecan Spark 10 M). Assay buffer was used as the negative control, and all assays were performed at least three times.

Confocal imaging of intracellular distribution

Coumarin was used to label $\mathbf{OP_{c3}}$ to obtain fluorescently labeled $\mathbf{OP_{c3}}$. $\mathbf{OP_{c3}}$-Coumarin (4 μg/mL) was incubated with NIH/3T3 cells in DMEM supplemented with 10 % FBS for 24 h or with *A. baumannii* in PBS for 8 h. The medium was then removed and the cells were washed three times with PBS. The cells (or bacteria) were then stained in PBS with Acridine Orange (5 μg/mL) for 20 min at 37 ◦C. After the bacteria and cells were washed three times with PBS, 1 mL of 4 % para-formaldehyde fixing solution was added. The resulting cultures were incubated for 30 min at 37 ◦C. Finally, the paraformaldehyde was replaced with appropriate amount of PBS after washed three times with PBS. Samples were imaged with Nikon A1R MP confocal microscope. The distribution of the drug in the cells and bacteria were analyzed by co-localization of green (AO) and blue (Hoechst) fluorescence.

ROS generation assay

S. aureus was cultured overnight in 4 mL CAMHB at 37 ◦C, and the bacteria were washed three times and re-suspended in PBS. The suspension was diluted to OD_{600nm} = 0.1, mixed with 10 μM 2,7-dichloro-fluorescein diacetate (DCFH-DA), and used as the working solution. Bacteria were placed into a 96-well plate (200 μL per well) and treated with **OP_{c3}** at 8 μg/mL for 3 h at 37 ◦C, in the dark. The ROS analysis was performed immediately by using flow cytometry (For DCFH-DA: Ex = 488 nm ± 30 nm, Em = 533 ± 30 nm.

Docking assay

We docked a fragment of **OP_{c3}** (includes four pyridinium) to $(CGCGAATTCGCG)_2$ using the x-ray crystallographic structure (4U8A) [37]. The receptor was prepared by setting the receptor docking grid center to the original ligand with a diameter of 10 to 12 Å in the crystal structure. Self-docking of the original ligand was carried out as a preliminary test of the ability of the receptor grid center to recover the crystallographic pose of the ligand. The protonation state of **OP_{c3}** was determined by using the "wash" function in Molecular Operating Environment (MOE) at pH = 7.3 was prepared by using the "Prepare Ligands" function in Discovery Studio 2.55 using all possible tautomers and stereoisomers generated. Docking was carried out using the CDOCKER module in Discovery Studio 2.55.

Dormant bacteria killing assay

Log-phase culture of GFP-*S. a* was added to DMEM with 10 % FBS at the concentration of 5×10^7 CFU/mL. The cells treated with **OP_{c3}** or Vancomycin were incubated at 37 ◦C and 220 rpm for 16–20 h. Bacterial load was determined through plating a 5 μL aliquot with series of 10-fold dilution onto agar plates and CFUs were counted after incubation for 10 h at 37 ◦C. Experiments were carried out in duplicate.

Bacterial persister killing assay

Persistent GFP-*S. a* was generated by treating the bacterial suspensions with 20 μg/mL Vancomycin. In brief, 1×10^8 CFU/mL GFP-*S. a* were treated with Erythromycin (15 μg/mL) and Vancomycin (20 μg/mL) for 6 h. Subsequently, **OP_{c3}** and Vancomycin at various concentrations was added. At each designated time point, an aliquot (10 μL) of the suspension was diluted by 10-fold serial dilution and then plated onto LB agar plates. After 16 h of cultivation at 37 ◦C, colonies were counted. The CFU/mL was calculated.

Time-kill assay

An overnight starter culture of bacteria in CAMHB was diluted 1000- fold in the same media and grown at 37 ◦C to reach an OD_{600nm} of approximately 0.3. This log-phase culture was then diluted into CAMHB to generate the working solution containing bacteria (5×10^5 CFU/mL). The working solution was treated with serially diluted compounds of interest, and the time at which each compound was added was defined as 0 h. At each designated time point, aliquots of the suspension (10 μL) were 10-fold serially diluted and plated onto LB agar plates. After overnight cultivation at 37 ◦C, colonies were counted, and CFU per milliliter was calculated.

Multistep resistance generation evaluation

The method for multistep resistance evolution was adapted from a reported procedure [22]. Briefly, the broth microdilution method for MIC determination against *S. aureus* and *E. coli* K12 were repeated for over 15 days. The initial inoculum was 5×10^5 CFU/mL in CAMHB. For each subsequent passage, the inoculum for MIC determination was adjusted to a final density of approximately 5×10^5 CFU/mL using the contents of a well containing compounds at a sub-inhibitory concentration (at which bacterial growth was observed from the previous passage). To measure the MIC of each passage, bacteria were transferred

to a new 96-well microtiter plate. Compounds were added in triplicate to wells in the first row of the microtiter plate

and then serially diluted. The plate was incubated at 37 ◦C for a minimum of 24 h before the MIC was determined by reading OD_{600} values. Resistance was classified as a greater than a 4-fold increase in the initial MIC.

Ex vivo and in vivo models

Hemolytic assay

Fresh ovine red blood cells were obtained and subjected to 25-fold dilution with PBS buffer to reach a concentration of approximately 4 % (in volume) of the blood cells. This red blood cell suspension was treated with serial dilutions of $\mathbf{OP_{c3}}$ in volume of 150 µL and further incubated at 37 ◦C for 1 h to allow for the hemolysis process to take place. At the end of the incubation time, the non-hemolyzed red blood cells were separated by centrifugation at 160 g for 10 min. Aliquots (100 µL) of the supernatant were transferred to a 96-well plate, and hemoglobin release was measured by UV-absorbance at 405 nm. Two controls were provided in this assay: an untreated red blood cell suspension in PBS solution was used as the negative control; a solution containing red blood cells lysed with 1 % triton-X was used as the positive control. Percentage of hemolysis was calculated using the following formula: Hemolysis (%) = [(OD_{405nm} of the treated sample - OD_{405nm} of the negative control)/ (OD_{405nm} of positive control - OD_{405nm} of negative control)] × 100 %.

MTT assay

Cells were seeded into 96-well plates (BIOFIL, catalog number TCP- 011–096) at 1×10^4 cells per well and incubated for 12 h in a cell incubator. Subsequently, cells were treated with different concentrations of various compounds in DMEM with 10 % FBS and then incubated for 24 h. Cells with no added compounds were used as controls. After 24 h, DMEM media was removed, cells were washed once with PBS, and then 120 µL of fresh medium containing MTT 0.5 mg/mL was added. Cells were further incubated in a 37 ◦C incubator for 1.5 h. After that, the DMEM media was replaced with 100 µL of DMSO, and cell viability was determined by measuring the absorbance at 595 nm. Cell viability values were expressed as percentages and calculated as follows: Viability % = (Abs (595 nm) of treated sample) / (Abs (595 nm) of control) × 100%.

Toxicity in mice

To assess the *in vivo* toxicity of $\mathbf{OP_{C3}}$, male ICR mice (6 to 8 weeks old, weighing 25 g each) were divided into two groups: a PBS treatment group (10 mg/kg, N = 2) and an $\mathbf{OP_{C3}}$ treatment group (10 mg/kg, N = 3). They were intraperitoneally injected with a single dose of $\mathbf{OP_{C3}}$ (10 mg/kg) daily for 7 days. The mice were weighed daily and observations were continued for an additional 7 days after the seventh injection.

Fibroblast biofilm infection model

A total of 5×10^4 NIH/3T3 cells were cultured in Dulbecco's modified Eagle medium (DMEM) with 10 % FBS at 37 ◦C in a humidified atmosphere of 5 % CO_2. Cells were maintained for 24 h to reach a confluent monolayer. Bacteria (GFP-*S. a*) were inoculated and harvested as mentioned above. Afterward, seeding solutions with 5×10^6 CFU/mL GFP-*S. a* were inoculated in buffered DMEM supplemented with 10 % FBS. The original medium was removed from 3 T3 cells followed by addition of 100 µL of seeding solution. The cocultures were then stored in a box humidified with damp paper towels at 37 ◦C overnight without shaking. Then, the original medium was removed from 3 T3 cells and replaced with serially diluted drugs. The cocultures were then stored in a box humidified with damp paper towels at 37 ◦C overnight without shaking. After 24 h, imaging was performed with an inverted fluorescence microscope.

Toxicity test of zebrafish

Zebrafish purchased from the animal market were reared in the laboratory for a week to adapt to the environment, and then 30 zebra- fishes were divided into 2 groups of 10 each. Each zebrafish was rescued by intraperitoneal injection of 2 μL of different drugs, and the PBS group was used as a control. The zebrafish were cultured in a tank containing pure water and the survival rate was observed.

Zebrafish infection model

This animal study was performed in accordance with national regulations on animal studies. The purchased zebrafish were maintained in the lab for a week prior to starting the experiment. In the experiment, 30 zebrafishes were divided into 3 groups for different treatments. To establish a bacterial infection model, each zebrafish was infected with 10^8 CFU *S. aureus* via intraperitoneal injection. After 30 min, 10 mg/kg **OP$_{c3}$**, 10 mg/kg Vancomycin via intraperitoneal injection. Control groups were injected with 2 μL of PBS. The treated fish were cultured in fresh ddH_2O for observation.

Antimicrobial efficacy evaluation on mice excision wound model

This animal study was conducted in accordance with national regulations for animal studies. The protocol was based on previously re- ported procedures with modifications [51]. Sixteen adult male ICR mice (6 to 8 weeks old, weighing 18 to 25 g each) were anesthetized with an intraperitoneal injection of chloral hydrate (70 mg/kg). An open excision wound (2 to 3 cm^2) was created on the dorsal skin of each mouse, reaching the depth of loose subcutaneous tissue. To establish the wound infection model, *S. aureus* suspensions (10^8 CFU) were inoculated on the excision wound area. Mice were divided into three groups: a PBS treatment group (N = 6), a **OP$_{c3}$** treatment group (10 mg/kg, N = 5), and a Vancomycin treatment group (10 mg/kg, N = 6). Treatments started 24 h post-infection, with 60 μL of compound solutions or PBS applied to the wound area and repeated every 24 h for 7 days. On every consecutive day for seven days, surviving mice had their wound surface bacterial load determined by wiping the wound with a sterile cotton swipe transferred to PBS, which was then plated on agar plates (supplemented with 20 μg/mL of Nalidixic acid) for CFU determination. Wound observations were conducted every 24 h, and the survival rate, wound healing rate, and weight change of each group were recorded over 14 days.

Funding sources

The funding support from the National Key Research and Development Program of China (2023YFD1800100 to X.F. and Y. B), National Natural Science Foundation of China (Grants 22177031 to X.F., 21877033 and 92163127 to Y.B., 82102415 to M.W., 82102408 to H.Y., 82304277 to C.Z.), Huxiang Youth Talent Support Program of Hunan Province (2022RC1107 to Y.B.), the Independent Research Project of the College of Advanced Interdisciplinary Studies of NUDT (22-ZZKY-03 to H.P.), the Health and Medical Research Fund (HMRF), Hong Kong SAR (22210412 to W.L.W.), Hunan Provincial Innovation Foundation For Postgraduate (QL20220075 to J. L.), China Postdoctoral Science Foundation (2022 M712681 to H.Y.) and Xuzhou Medical University Excel- lent Talent Introduction Project (D2019030 to H.Y.) are gratefully acknowledged.

Declaration of competing interest

The authors declare that they have no known competing financial interests or personal relationships that could have appeared to influence the work reported in this paper.

References

[1] M. Jamal, W. Ahmad, S. Andleeb, F. Jalil, M. Imran, M.A. Nawaz, T. Hussain, M. Ali, M. Rafiq, M.A. Kamil, Bacterial biofilm and associated infections, J. Chin. Med. Assoc. 81 (1) (2018) 7–11.

[2] D. Davies, Understanding biofilm resistance to antibacterial agents, Nat. Rev. Drug Discov. 2 (2) (2003) 114–122.

[3] K. Lewis, Riddle of biofilm resistance, Antimicrob. Agents Chemother. 45 (4) (2001) 999–1007.

[4] A.K. Epstein, B. Pokroy, A. Seminara, J. Aizenberg, Bacterial biofilm shows persistent resistance to liquid wetting and gas penetration, PNAS 108 (3) (2011) 995–1000.

[5] H.-C. Flemming, E.D. van Hullebusch, T.R. Neu, P.H. Nielsen, T. Seviour, P. Stoodley, J. Wingender, S. Wuertz, The biofilm matrix: multitasking in a shared space, Nat. Rev. Microbiol. 21 (2) (2023) 70–86.

[6] A.D. Verderosa, M. Totsika, K.E. Fairfull-Smith, Bacterial Biofilm Eradication Agents: A Current Review, Front. Chem. 7 (2019) 824.

[7] L. Karygianni, Z. Ren, H. Koo, T. Thurnheer, Biofilm matrixome: extracellular components in structured microbial communities, Trends Microbiol. 28 (8) (2020) 668–681.

[8] K.P. Rumbaugh, K. Sauer, Biofilm dispersion, Nat. Rev. Microbiol. 18 (10) (2020) 571–586.

[9] H. Koo, R.N. Allan, R.P. Howlin, P. Stoodley, L. Hall-Stoodley, Targeting microbial biofilms: current and prospective therapeutic strategies, Nat. Rev. Microbiol. 15 (12) (2017) 740–755.

[10] H.-C. Flemming, J. Wingender, U. Szewzyk, P. Steinberg, S.A. Rice, S. Kjelleberg, Biofilms: an emergent form of bacterial life, Nat. Rev. Microbiol. 14 (9) (2016) 563–575.

[11] H. Van Acker, P. Van Dijck, T. Coenye, Molecular mechanisms of antimicrobial tolerance and resistance in bacterial and fungal biofilms, Trends Microbiol. 22 (6) (2014) 326–333.

[12] P.S. Stewart, B. White, L. Boegli, T. Hamerly, K.S. Williamson, M.J. Franklin, B. Bothner, G.A. James, S. Fisher, F.G. Vital-Lopez, A. Wallqvist, Conceptual model of biofilm antibiotic tolerance that integrates phenomena of diffusion, metabolism, gene expression, and physiology, J. Bacteriol. 201 (22) (2019) e00307–e319.

[13] R. Roy, M. Tiwari, G. Donelli, V. Tiwari, Strategies for combating bacterial biofilms: a focus on anti-biofilm agents and their mechanisms of action, Virulence 9(1) (2018) 522–554.

[14] H. Ceri, M.E. Olson, C. Stremick, R.R. Read, D. Morck, A. Buret, The calgary biofilm device: new technology for rapid determination of antibiotic susceptibilities of bacterial biofilms, J. Clin. Microbiol. 37 (6) (1999) 1771–1776.

[15] D. Lebeaux, J.-M. Ghigo, C. Beloin, Biofilm-related infections: bridging the gap between clinical management and fundamental aspects of recalcitrance toward antibiotics, Microbiol Mol Biol Rev 78 (3) (2014) 510–543.

[16] L. Matilla-Cuenca, C. Gil, S. Cuesta, B. Rapun-Araiz, M. Ziemyte, A. Mira, I. Lasa, J. Valle, Antibiofilm activity of flavonoids on staphylococcal biofilms through targeting BAP amyloids, Sci. Rep. 10 (1) (2020) 18968.

[17] Z.Y. Ong, S.J. Gao, Y.Y. Yang, Short syntheticβ-sheet forming peptide amphiphiles as broad spectrum antimicrobials with antibiofilm and endotoxin neutralizing capabilities, Adv. Funct. Mater. 23 (29) (2013) 3682–3692.

[18] T.K. Nguyen, S.J. Lam, K.K. Ho, N. Kumar, G.G. Qiao, S. Egan, C. Boyer, E.H. Wong, Rational design of single-chain polymeric nanoparticles that kill planktonic and biofilm bacteria, ACS Infect. Dis. 3 (3) (2017) 237–248.

[19] R. Liu, X. Chen, S.P. Falk, K.S. Masters, B. Weisblum, S.H. Gellman, Nylon-3 polymers active against drug-resistant Candida albicans biofilms, J. Am. Chem. Soc. 137 (6) (2015) 2183–2186.

[20] S. Tian, L. Su, Y. Liu, J. Cao, G. Yang, Y. Ren, F. Huang, J. Liu, Y. An, H.C. van der Mei, H.J. Busscher, L. Shi, Self-targeting, zwitterionic micellar dispersants enhance antibiotic killing of infectious biofilms-an intravital imaging study in mice, Sci. Adv. 6 (33) (2020) eabb1112.

[21] J. Zhang, H. Wu, D. Wang, L. Wang, Y. Cui, C. Zhang, K. Zhao, L. Ma, G. Pier, Intracellular glycosyl hydrolase PslG shapes bacterial cell fate, signaling, and the biofilm development of Pseudomonas aeruginosa, Elife 11 (2022) e72778.

[22] S. Bai, J. Wang, K. Yang, C. Zhou, Y. Xu, J. Song, Y. Gu, Z. Chen, M. Wang, C. Shoen, B. Andrade, M. Cynamon, K. Zhou, H. Wang, Q. Cai, E. Oldfield, S.C. Zimmerman, Y. Bai, X. Feng, A polymeric approach toward resistance-resistant antimicrobial agent with dual-selective mechanisms of action, Sci. Adv. 7(5) eabc9917.

[23] Z. Chen, W. Zhang, Y. Chen, Y. Wang, S. Bai, Q. Cai, H. Pu, Z. Wang, X. Feng, Y. Bai, Alternatingly amphiphilic antimicrobial oligoguanidines:structure-property relationship and usage as the coating materialwith unprecedented hemocompatibility, Chem. Mater. 34 (8) (2022) 3670–3682.

[24] G. Huang, H. Shen, X. Chen, T. Wu, Z. Chen, Y. Chen, J. Song, Q. Cai, Y. Bai, H. Pu, X. Feng, A degradable, broad-spectrum and resistance-resistant antimicrobial oligoguanidine as a disinfecting and therapeutic agent in aquaculture, Polym. Chem. 13 (23) (2022) 3539–3551.

[25] X. Chen, C. Zhou, J. Wang, T. Wu, E. Lei, Y. Wang, G. Huang, Y. Yu, Q. Cai, H. Pu, X. Feng, Y. Bai, Improving the hemocompatibility of antimicrobial peptidomimetics through amphiphilicity masking using a secondary amphiphilic polymer, Adv. Healthc. Mater. 11 (15) (2022) 2200546.

[26] C. Zhou, Y. Zhou, Y. Zheng, Y. Yu, K. Yang, Z. Chen, X. Chen, K. Wen, Y. Chen, S. Bai, J. Song, T. Wu, E. Lei, M. Wan, Q. Cai, L. Ma, W.-L. Wong, Y. Bai, C. Zhang, X. Feng, Amphiphilic nano-swords for direct penetration and eradication of pathogenic bacterial biofilms, ACS Appl. Mater. Interfaces 15 (16) (2023) 20458–20473.

[27] J. Wang, J. Song, X. Chen, R.-T. Guo, Y. Wang, G. Huang, N. Zheng, P. Hu, X. Feng, Y. Bai, Multivalent display of lipophilic DNA binders for dual-selective anti- mycobacterium peptidomimetics with binary mechanism of action, CCS Chem. 4(11) (2022) 3573–3586.

[28] V.D. Sharma, E.O. Aifuwa, P.A. Heiney, M.A. Ilies, Interfacial engineering of pyridinium gemini surfactants for the generation of synthetic transfection systems, Biomaterials 34 (28) (2013) 6906–6921.

[29] M.J. Matos, C.D. Navo, T. Hakala, X. Ferhati, A. Guerreiro, D. Hartmann, B. Bernardim, K.L. Saar, I. Compan˜o´n, F. Corzana, T.P.J. Knowles, G. Jim´enez-Os´es, G.J.L. Bernardes, Quaternization of vinyl/alkynyl pyridine enables ultrafast cysteine-selective protein modification and charge modulation, Angew. Chem. Int. Ed. 58 (20) (2019) 6640–6644.

[30] Z. Geng, M.G. Finn, Thiabicyclononane-based antimicrobial polycations, J. Am. Chem. Soc. 139 (43) (2017) 15401–15406.

[31] V. Sambhy, B.R. Peterson, A. Sen, Antibacterial and hemolytic activities of pyridinium polymers as a function of the spatial relationship between the positive charge and the pendant alkyl tail, Angew. Chem. Int. Ed. 47 (7) (2008) 1250–1254.

[32] R.F. Epand, P.B. Savage, R.M. Epand, Bacterial lipid composition and the antimicrobial efficacy of cationic steroid compounds (Ceragenins), BBA- Biomembranes 1768 (10) (2007) 2500–2509.

[33] V.A.K. Rathinam, Y. Zhao, F. Shao, Innate immunity to intracellular LPS, Nat. Immunol. 20 (5) (2019) 527–533.

[34] T. Mourer, M. El Ghalid, G. Pehau-Arnaudet, B. Kauffmann, A. Loquet, S. Brule, V. Cabral, C. d'Enfert, S. Bachellier-Bassi, The Pga59 cell wall protein is an amyloid forming protein involved in adhesion and biofilm establishment in the pathogenic yeast candida albicans, npj Biofilms Microbiomes 9 (1) (2023) 6.

[35] P. Di Martino, Bap: a new type of functional amyloid, Trends Microbiol. 24 (9) (2016) 682–684.

[36] Y. Jiang, M. Han, Y. Bo, Y. Feng, W. Li, J.R. Wu, Z. Song, Z. Zhao, Z. Tan, Y. Chen, T. Xue, Z. Fu, S.H. Kuo, G.W. Lau, E. Luijten, J. Cheng, "Metaphilic" cell- penetrating polypeptide-vancomycin conjugate efficiently eradicates intracellular bacteria via a dual mechanism, ACS Cent. Sci. 6 (12) (2020) 2267–2276.

[37] M.A. Kohanski, D.J. Dwyer, B. Hayete, C.A. Lawrence, J.J. Collins, A common mechanism of cellular death induced by bactericidal antibiotics, Cell 130 (5) (2007) 797–810.

[38] D.J. Dwyer, P.A. Belenky, J.H. Yang, I.C. MacDonald, J.D. Martell, N. Takahashi, C. T.Y. Chan, M.A. Lobritz, D. Braff, E.G. Schwarz, J.D. Ye, M. Pati, M. Vercruysse, P. S. Ralifo, K.R. Allison, A.S. Khalil, A.Y. Ting, G.C. Walker, J.J. Collins, Antibiotics induce redox-related physiological alterations as part of their lethality, PNAS 111 (20) (2014) E2100–E2109.

[39] E. Lei, H. Tao, S. Jiao, A. Yang, Y. Zhou, M. Wang, K. Wen, Y. Wang, Z. Chen, X. Chen, J. Song, C. Zhou, W. Huang, L. Xu, D. Guan, C. Tan, H. Liu, Q. Cai, K. Zhou, J. Modica, S.-Y. Huang, W. Huang, X. Feng, Potentiation of vancomycin: creating cooperative membrane lysis through a "derivatization-for-sensitization" approach, J. Am. Chem. Soc. 144 (23) (2022) 10622–10639.

[40] J. Zhang, T. Lu, Efficient evaluation of electrostatic potential with computerized optimized code, PCCP 23 (36) (2021) 20323–20328.

[41] W. Zhu, Y. Wang, K. Li, J. Gao, C.-H. Huang, C.-C. Chen, T.-P. Ko, Y. Zhang, R.-T. Guo, E. Oldfield, Antibacterial drug leads: DNA and enzyme multitargeting, J. Med. Chem. 58 (3) (2015) 1215–1227.

[42] J. Yan, B.L. Bassler, Surviving as a community: antibiotic tolerance and persistence in bacterial biofilms, Cell Host Microbe 26 (1) (2019) 15–21.

[43] T.K. Wood, S.J. Knabel, B.W. Kwan, Bacterial persister cell formation and dormancy, Appl. Environ. Microbiol. 79 (23) (2013) 7116–7121.

[44] J.M. Stokes, K. Yang, K. Swanson, W. Jin, A. Cubillos-Ruiz, N.M. Donghia, C. R. MacNair, S. French, L.A. Carfrae, Z. Bloom-Ackerman, V.M. Tran, A. Chiappino- Pepe, A.H. Badran, I.W. Andrews, E.J. Chory, G.M. Church, E.D. Brown, T. S. Jaakkola, R. Barzilay, J.J. Collins, A deep learning approach to antibiotic discovery, Cell 180 (4) (2020) 688–702.

[45] M.A. Kohanski, D.J. Dwyer, J.J. Collins, How antibiotics kill bacteria: from targets to networks, Nat. Rev. Microbiol. 8 (6) (2010) 423–435.

[46] K. Lewis, Persister cells, dormancy and infectious disease, Nat. Rev. Microbiol. 5(1) (2007) 48–56.

[47] M.H. Muhammad, A.L. Idris, X. Fan, Y. Guo, Y. Yu, X. Jin, J. Qiu, X. Guan, T. Huang, Beyond risk: bacterial biofilms and their regulating approaches, Front. Microbiol. 11 (2020) 928.

[48] C. Beloin, A. Roux, J.M. Ghigo, Escherichia coli biofilms, in: T. Romeo (Ed.), Bacterial Biofilms2008, pp. 249-289.

[49] J.-H. Ch'ng, K.K.L. Chong, L.N. Lam, J.J. Wong, K.A. Kline, Biofilm-associated infection by enterococci, Nat. Rev. Microbiol. 17 (2) (2019) 82–94.

[50] M.Z. David, R.S. Daum, Community-associated methicillin-resistant staphylococcus aureus: epidemiology and clinical consequences of an emerging epidemic, Clin. Microbiol. Rev. 23 (3) (2010) 616–687.

[51] J. Hoque, M.M. Konai, S.S. Sequeira, S. Samaddar, J. Haldar, Antibacterial and antibiofilm activity of cationic small molecules with spatial positioning of hydrophobicity: an in vitro and in vivo evaluation, J. Med. Chem. 59 (23) (2016) 10750–10762.

[52] I. Wiegand, K. Hilpert, R.E.W. Hancock, Agar and broth dilution methods to determine the minimal inhibitory concentration (MIC) of antimicrobial substances, Nat. Protoc. 3 (2) (2008) 163–175.

[53] D.-Y. Wang, L. Su, G. Yang, Y. Ren, M. Zhang, H. Jing, X. Zhang, R. Bayston, H. C. van der Mei, H.J. Busscher, L. Shi, Self-targeting of zwitterion-based platforms for nano-antimicrobials and nanocarriers, J. Mater. Chem. B 10 (14) (2022) 2316–2322.

[54] M. Xiong, M.W. Lee, R.A. Mansbach, Z. Song, Y. Bao, R.M. Peek Jr., C. Yao, L. F. Chen, A.L. Ferguson, G.C. Wong, J. Cheng, Helical antimicrobial polypeptides with radial amphiphilicity, PNAS 112 (43) (2015) 13155–13160.

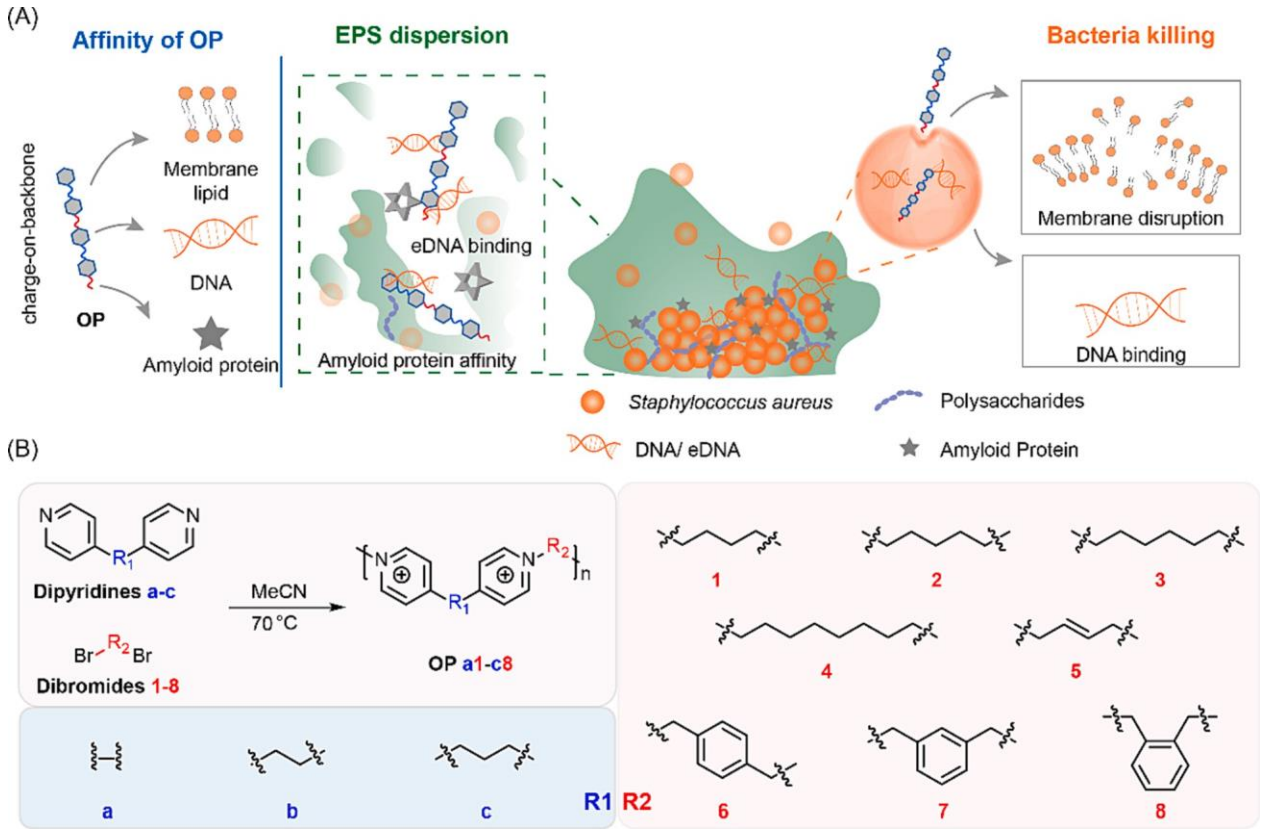

Fig. 1. Design of oligopyridiniums (**OPs**) and their effects in bacterial biofilm inhibition and eradication. (A) Affinity of $\mathbf{OP_{c3}}$ to biomacromolecules, and its effects in EPS dispersion and bacteria killing. (B) Synthesis and structures of **OP** library.

Table 1. The antimicrobial activity of pyridinium-based oligomers (MIC, μg/mL) against various bacteria including laboratory strains and clinical isolates with multidrug resistance: *Escherichia coli* (*E. c*); *Acinetobacter baumannii* (*A. b*); *Staphylococcus aureus* (*S. a*); *Bacillus subtilis* (*B. s*); *Enterococcus faecalis* (*E. f*). GFP-harboring strain of *Staphylococcus aureus* (GFP-*S. a*).

OP	MIC [1]						MBIC [2]	MBEC [3]
	Gram-negative			Gram-positive				
	E. c	*E. c*-c [4]	*A. b*	*S. a*	*B. s*	*E. f*	GFP-*S.a*	GFP-*S.a*
a1	4	4	4	1	2	2	32	64
a2	4	2	2	0.5	<0.5	2	32	64
a3	2	2	2	1	<0.5	2	32	64
a4	2	4	4	2	2	2	64	128
a5	2	2	2	1	<0.5	2	>128	>128
a6	4	1	2	1	<0.5	8	32	64
a7	4	4	4	2	4	8	64	128
a8	8	8	8	4	2	8	64	>128
b1	4	2	2	0.5	<0.5	1	32	64
b2	4	4	8	1	2	2	32	128
b3	2	2	2	1	<0.5	1	64	64
b4	8	1	2	1	1	1	32	32
b5	4	1	2	0.5	<0.5	2	32	128
b6	4	4	8	2	4	8	128	>128
b7	4	4	8	2	2	2	32	128
b8	4	4	8	2	2	2	32	128
c1	4	4	2	2	<0.5	1	16	64
c2	2	2	2	1	<0.5	1	8	64
c3	2	2	2	1	<0.5	1	8	16
c4	<1	1	0.5	0.5	<0.5	1	4	32
c5	<1	1	2	0.5	<0.5	1	8	64
c6	8	8	8	8	2	8	8	32
c7	2	1	2	2	<0.5	1	16	64
c8	4	4	8	8	4	2	32	>128

[1] Minimum Inhibitory Concentration; [2] Minimum Biofilm Inhibition Concentration; [3] Minimum Biofilm Eradication Concentration; [4] Strain having its name ending with -c is clinical isolate with multidrug resistance.

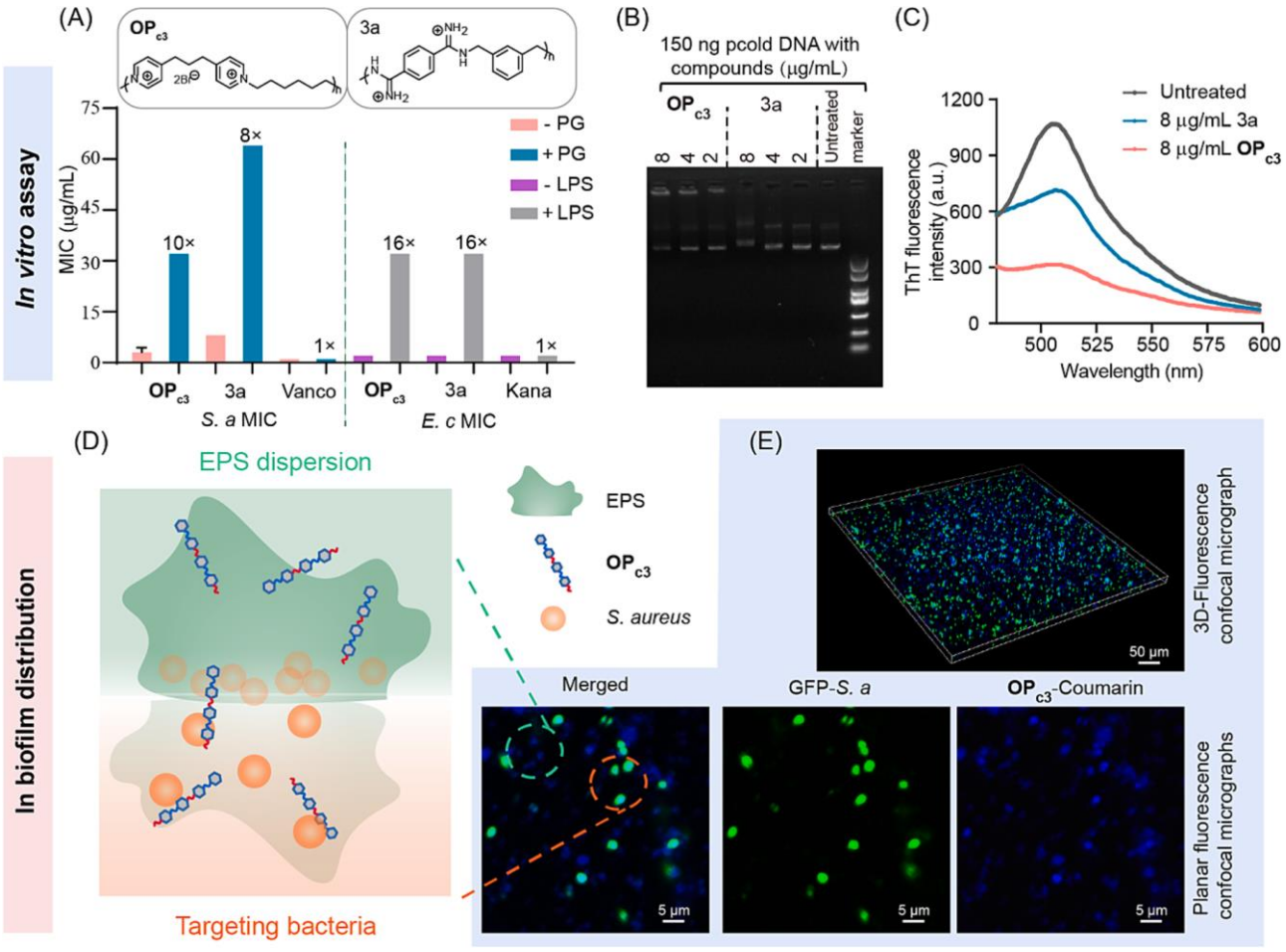

Fig. 2. The affinity of **OPc3** to biological macromolecules and its distribution within biofilms *in vitro*. (A) The effect of exogenous PG and LPS on the MIC of **OPc3**, Kanamycin (Kana), and Vancomycin (Vanco) against *S. aureus* or *E. coli*. And structures of **OPc3** and 3a. (B) Gel retardation assay using **OPc3** and a plasmid DNA labelled with Gel-Red, showing that **OPc3** could retard DNA migration and displace Gel-Red. (C) ThT fluorescence intensity of amyloid fiber, treated with **OPc3** and **3a** as measured by fluorometer. (D) Illustration of biofilm distribution of **OPc3** through targeting extracellular polymeric substances (EPS) and within bacterial cells. (E) Visualization of co-localization of coumarin-labelled **OPc3** with both GFP-*S. a* EPS matrix within the biofilm after treatment with 64 μg/mL **OPc3**-Coumarin for 24 h.

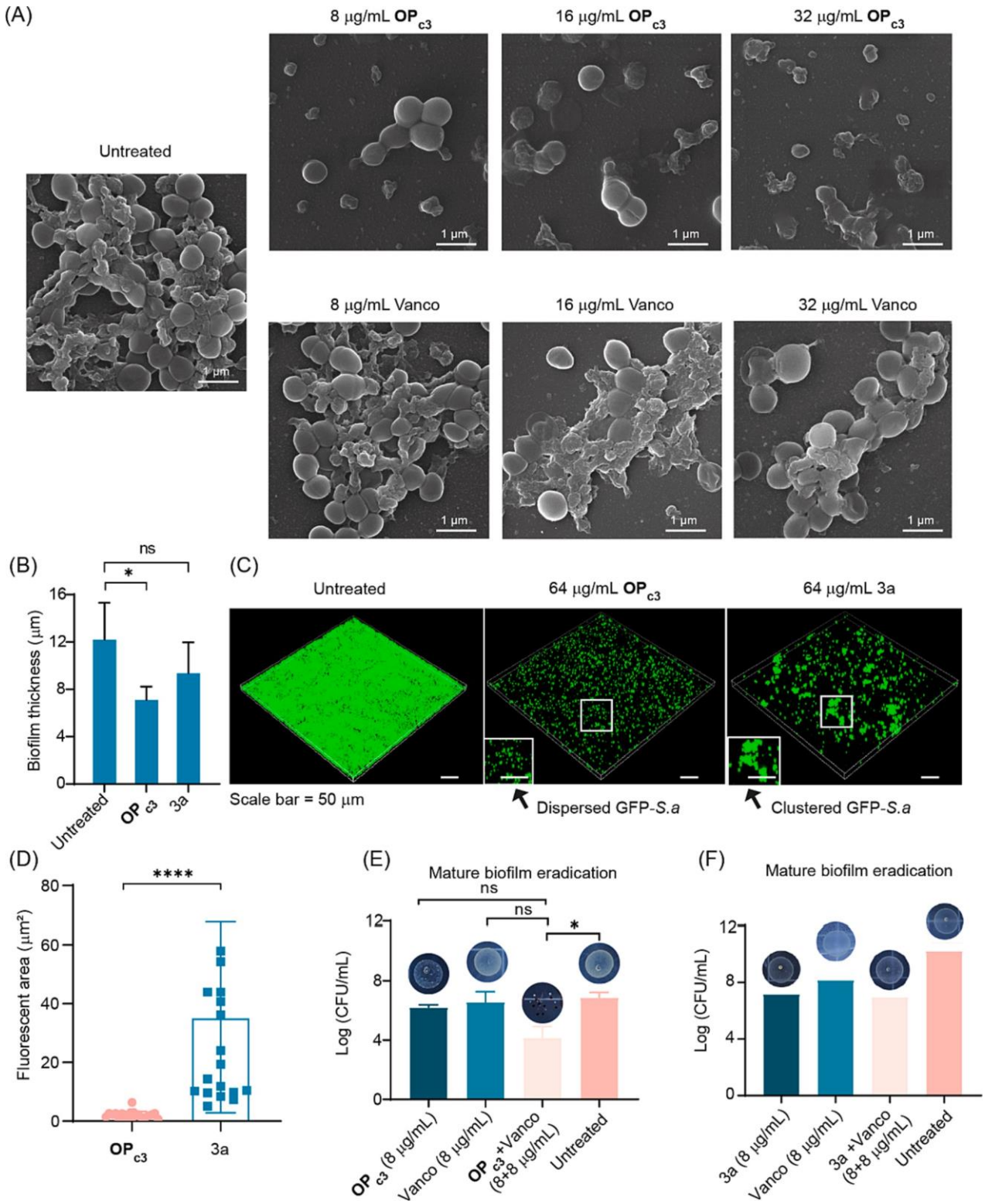

Fig. 3. OP_{c3} exhibited effective destruction of mature biofilms**.** (A) Microscopic visualization of eradication activity of **OP_{c3}** and Vancomycin against GFP-*S. a* biofilm by SEM. (B) Thickness of GFP-*S. a* biofilm after exposure to **OP_{c3}** or 3a suspensions. (C) 3D-Fluorescence confocal micrographs of mature GFP-*S. a* biofilm treated with 64 μg/mL **OP_{c3}** and 3a. (D) Fluorescence area analysis of 20 selected points from 3D confocal images of biofilms using Image J. (E) Quantification of the synergistic effect between **OP_{c3}** and Vancomycin in the biofilm eradication. (F) Quantification of the synergistic effect between 3a and Vancomycin in the biofilm checkboard study. (Statistical significances were analyzed using student's *t*-test and significant differences between groups are marked with an asterisk. ns, **, *** and **** indicate $P > 0.05$, $P \leq 0.01$, $P \leq 0.001$ and $P \leq 0.0001$, respectively.).

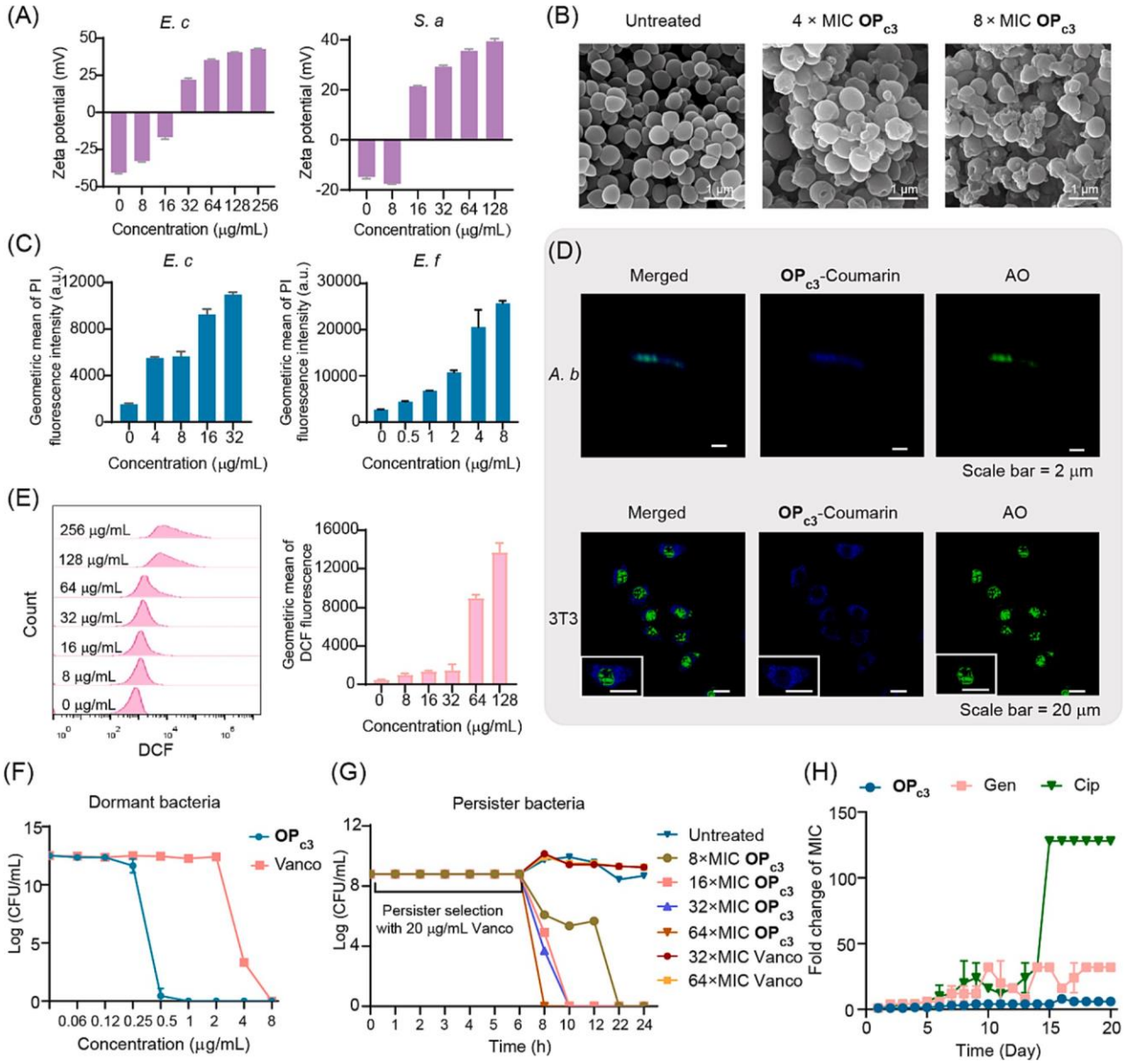

Fig. 4. Dual-targeting antimicrobial mechanism of **OP$_{c3}$** killing bacteria with different lifestyles. (A) Zeta potential measurement of *E. coli* and *S. aureus* in the presence of different concentrations of **OP$_{c3}$**. Increase in bacterial surface potential suggests that **OP$_{c3}$** could accumulate on the bacterial membrane and effectively neutralize the negative charge of bacterial surface. (B) SEM images of untreated and **OP$_{c3}$**-treated GFP-*S. a*, displaying apparent membrane damage by **OP$_{c3}$**, with fragments and broken cells being observed. (MIC of **OP$_{c3}$** is 2 μg/mL) (C) Membrane permeability assays of *E. coli* and *E. faecalis* cells with propidium iodide (PI) staining to demonstrate the bacterial cell membrane disruption caused by the addition of **OP$_{c3}$**. (D) Visualization of intracellular localization of **OP$_{c3}$** in *A. baumannii* cells and in eukaryotic cells (NIH/3T3). (E) ROS generation by **OP$_{c3}$** at different concentrations in *S. aureus* probed by DCFH-DA. (F) The activity of **OP$_{c3}$** and Vancomycin (Vanco) at different concentrations against dormant bacteria (GFP-*S. a*) cultured in DMEM + 10 % FBS. (G) Killing kinetics against GFP-*S. a* persisters (induced with 20 μg/mL of Vanco) by **OP$_{c3}$** and Vanco. (H) Resistance evolution profiles for **OP$_{c3}$**, Gentamicin (Gen) and Ciprofloxacin (Cip) against *S. aureus*.

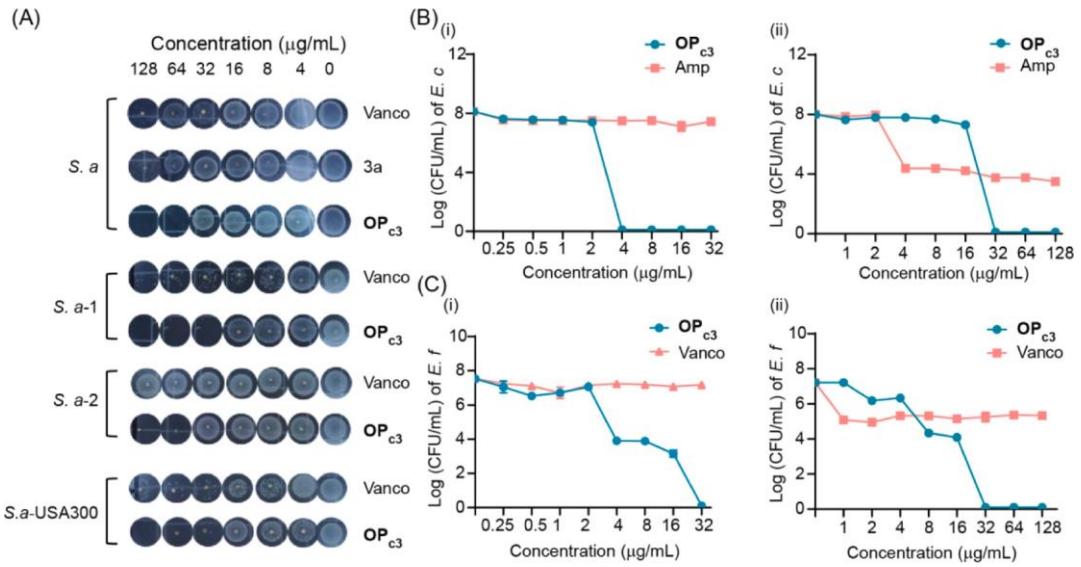

Fig. 5. Antibiofilm activities of **OP$_{c3}$** against clinically isolated *S. aureus* strains and other pathogenic bacteria. (A) Dose-dependent eradication effects of **OP$_{c3}$** against laboratory *S. aureus* (Newman, *S. a*) and other multi-drug resistant strains (*S. a*-1, *S. a*-2, *S. a*-USA300). (B) Effects of **OP$_{c3}$** against *E. coli* biofilm formation (i) and eradication (ii). (C) Effects of **OP$_{c3}$** against *E. faecalis* biofilm formation (i) and eradication (ii). (Amp: Ampicillin; Vanco: Vancomycin).

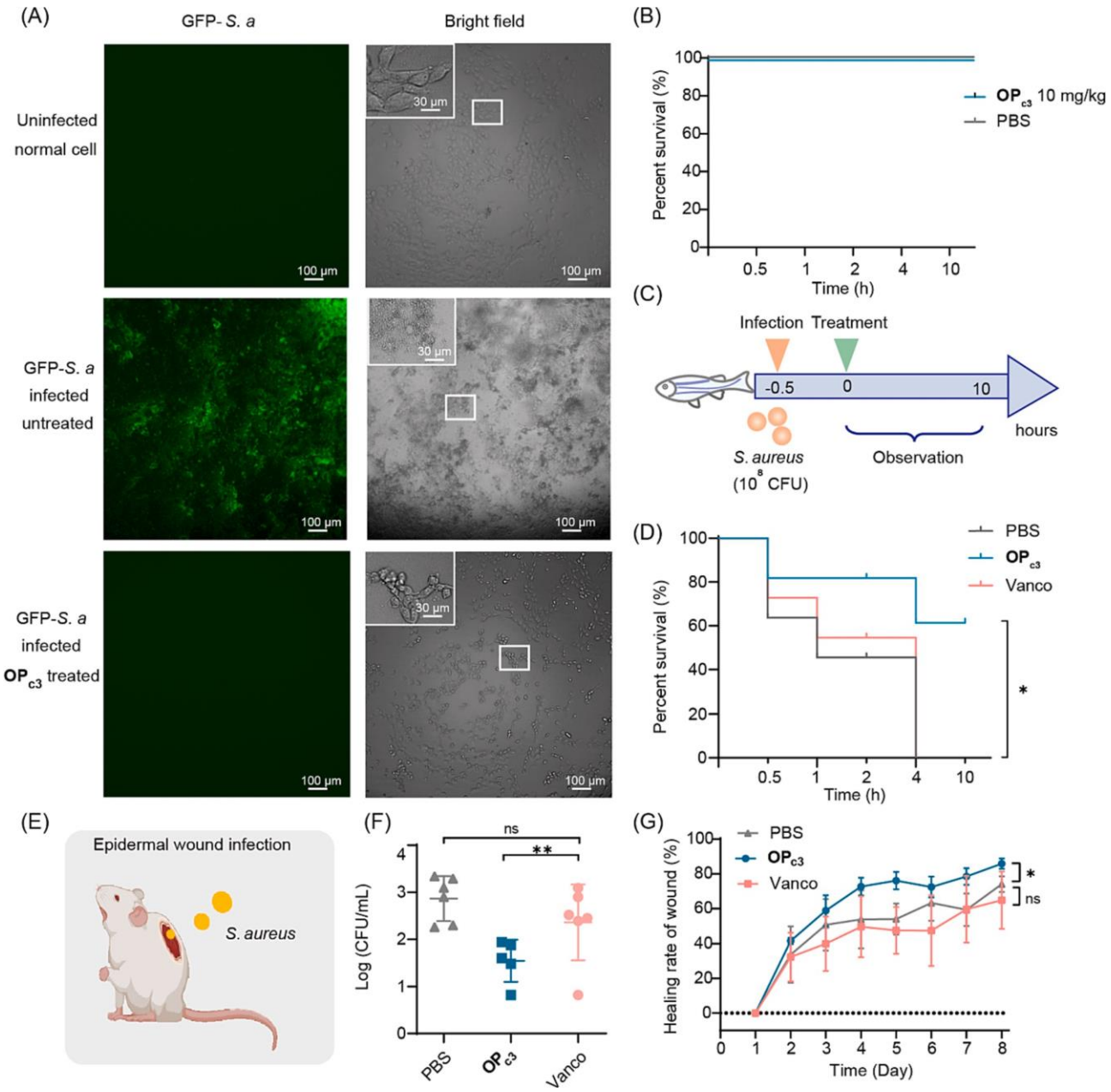

Fig. 6. Antibacterial effects of **OP$_{c3}$** in *ex vivo* and *in vivo* infection models. (A) Antibiofilm effects of **OP$_{c3}$** (4 μg/mL) and Vancomycin (4 μg/mL) in an *ex vivo* fibroblast biofilm infection model based on the NIH-3 T3 cell line, demonstrated through confocal images. (B) Survival analysis of zebrafish treated with PBS and 10 mg/kg **OP$_{c3}$**. (C) Scheme for zebrafish infection model treatment. (D) Survival analysis of *S. aureus*-infected zebrafish after different treatments (10 mg/kg **OP$_{c3}$**, 10 mg/kg Vancomycin and PBS). (E) Scheme depicting the *S. aureus* epidermal wound infection model. (F) The effects of **OP$_{c3}$** in reducing the bacterial biofilm load on wounds after one administration of the drug. (G) The effect of **OP$_{c3}$** in enhancing wound healing rate in the *S. aureus* infected mice. (Statistical significances were determined for the analysis on the seventh day post-treatment.).